

TOPICAL REVIEW

Measurement of the complex permittivity, initial permeability, permeability tensor and ferromagnetic linewidth of gyromagnetic materials

To cite this article: Jerzy Krupka 2018 *Meas. Sci. Technol.* **29** 092001

View the [article online](#) for updates and enhancements.

Related content

- [Frequency domain complex permittivity measurements at microwave frequencies](#)
- [Measurements of the complex permittivity of highly concentrated aqueous NaCl solutions and ferrofluid employing microwave cylindrical cavities](#)
- [Comparison of split post dielectric resonator and ferrite disc resonator techniques for microwave permittivity measurements of polycrystalline yttrium iron garnet](#)

Topical Review

Measurement of the complex permittivity, initial permeability, permeability tensor and ferromagnetic linewidth of gyromagnetic materials

Jerzy Krupka^{ID}

Institute of Microelectronics and Optoelectronics, Warsaw University of Technology, Warsaw 00662, Poland

E-mail: krupka@imio.pw.edu.pl

Received 8 April 2018, revised 28 May 2018

Accepted for publication 27 June 2018

Published 26 July 2018



Abstract

A review of the measurement methods of the basic electromagnetic parameters of gyromagnetic materials at microwave frequencies is presented. Measurement methods of the complex permittivity, the complex initial permeability, the intrinsic permeability tensor components and the ferromagnetic linewidth are considered. A large part of the paper is devoted to the description and analysis of the rigorous electrodynamic methods for extraction of the measured parameters from the raw measurement data. Four groups of gyromagnetic materials are considered: microwave magnetic absorbers, polycrystalline ferrites, low loss monocrystalline garnets and thin metallic ferromagnetic films. Measurement fixtures include resonant and non-resonant fixtures, employing resonance cavities, dielectric resonators and sections of transmission lines. A rigorous electrodynamic approach to data analysis allows us to improve the accuracy of the measurements to compare them to the commonly used perturbation methods.

Keywords: complex permittivity, initial permeability, permeability tensor, ferromagnetic linewidth

(Some figures may appear in colour only in the online journal)

1. Introduction

Magnetic materials, particularly ferrites, play a very important role in the construction of microwave devices and components. Microwave ferrites can be divided into groups, where different parameters are of interest, for the following applications:

- (1) Magnetically tunable devices such as filters, power limiters and oscillators. For such devices the lowest loss materials, such as pure or doped monocrystalline yttrium iron garnets (YIG), are used.

- (2) Microwave devices such as circulators, isolators and phase shifters. Such devices usually employ low loss polycrystalline ferrite materials, and they operate at frequencies that are higher than the natural frequency of ferromagnetic resonance f_m which is defined as $f_m = \gamma_{\text{eff}} M_s$ where M_s is the saturation magnetization of ferrite material, and γ_{eff} is the effective gyromagnetic ratio. The free electron gyromagnetic ratio is known with high precision from cyclotron measurements $\gamma_e = \frac{|e|}{2m_e} g_e \approx 35.21719 \text{ MHz } (\text{kA m}^{-1})^{-1}$, and the g -factor $g_e = 2.002\ 319$, while for real ferrite materials, g -factor values are determined from

experiments. The g -factor values for typical microwave ferrites are close to that for the electron g_e , therefore, it is often assumed that $\gamma_{\text{eff}} = \gamma_e = \gamma$.

- (3) Microwave absorbers. For this application magnetic materials that exhibit high magnetic losses at a frequency range of interest are used. They operate at frequencies below the natural frequency of the ferromagnetic resonance.

For the first group of devices the most important parameters are the ferromagnetic linewidth ΔH —the parameter related to the magnetic losses (or Q -factors)—and the range of tunability.

For the second and third groups, the parameters of interest are the complex permittivity and the complex permeability. While for some applications, e.g. for microwave absorbers, these parameters should be known in the demagnetized state, for the first and second groups they should be ideally measured as a function of the static magnetic field bias, and possibly for different microwave power levels.

In this paper a review of the microwave measurement methods of the complex permittivity, the initial complex permeability, the complex permeability tensor and the ferromagnetic linewidth is presented.

2. Basic definitions

In this section we introduce definitions of parameters that are to be measured or those that have an influence on the measured parameters.

2.1. Permittivity

At the frequency domain the complex permittivity is defined as a tensor quantity $\bar{\varepsilon}$ describing the relationship: $\mathbf{D} = \bar{\varepsilon}\mathbf{E}$ between the electric displacement \mathbf{D} and the electric field \mathbf{E} vectors.

For ferrites the permittivity tensor is symmetric and in a specific coordinate system it takes the diagonal form (1). Tensor elements can be in general complex quantities, and their imaginary parts describe the sum of the dielectric and conductor losses

$$\bar{\varepsilon} = \varepsilon_0 \begin{bmatrix} \varepsilon_{11} & 0 & 0 \\ 0 & \varepsilon_{22} & 0 \\ 0 & 0 & \varepsilon_{33} \end{bmatrix}. \quad (1)$$

For most ferrites all of the diagonal tensor elements in (1) are identical and the complex permittivity can be treated as a scalar quantity.

2.2. Permeability tensor

Similar to the complex permittivity, the complex permeability tensor $\bar{\mu}$ describes the relationship $\mathbf{B} = \bar{\mu}\mathbf{H}$ between the magnetic induction \mathbf{B} and the magnetic field \mathbf{H} vectors. The most important microwave applications of magnetic materials

at microwave frequencies are related to their non-reciprocal properties arising from the ferromagnetic resonance (FMR) phenomenon [1]. FMR can be quantitatively described with a permeability tensor that can be derived from the Landau–Lifshitz–Gilbert equation. In the presence of uniform static magnetic field magnetizing ferrite material along the z -axis of a Cartesian or cylindrical coordinate system, the permeability tensor takes the form (2). When the static magnetic field is sufficiently strong, to saturate the gyromagnetic medium, then $\mu_{||} = 1$ and the permeability tensor is known as the Polder's tensor [2]

$$\bar{\mu} = \mu_0 \begin{bmatrix} \mu & j\kappa & 0 \\ -j\kappa & \mu & 0 \\ 0 & 0 & \mu_{||} \end{bmatrix}. \quad (2)$$

The diagonal and the off-diagonal relative components of the Polder tensor take the following form [3]:

$$\mu = 1 + \frac{H_{0r} + j\alpha \hat{w}}{H_{0r}^2 - \hat{w}^2 + 2j\alpha H_{0r}\hat{w}} \quad (3)$$

$$\kappa = \frac{\hat{w}}{H_{0r}^2 - \hat{w}^2 + 2j\alpha H_{0r}\hat{w}} \quad (4)$$

where: $H_{0r} = H_0/M_S$, $\hat{w} = \hat{f}/f_m$, $f_m = \gamma M_S$, H_0 is the static magnetic field inside the sample (the internal static magnetic field), M_S is the saturation magnetization, α is a Gilbert damping factor, and \hat{f} is the complex frequency.

As will be shown later, the imaginary part of the frequency describes the time dependence of electromagnetic fields (transient solutions) for a microwave resonator containing lossy medium. As an alternative to the Gilbert damping factor the relaxation time, $\tau = 1/(\alpha\gamma H_0)$, and the FMR linewidth, $\Delta H = 2\alpha H_0 = 2/(\gamma\tau)$, are used to describe the losses in ferromagnetic material.

It should be emphasized that expressions (3) and (4) are valid if the ferromagnetic medium is fully magnetized, i.e. when $H_0 > M_S$ when the domain structure in ferromagnetic material vanishes.

For a circularly polarized electromagnetic (EM) field the permeability of ferromagnetic material biased with a static magnetic field, orthogonally polarized with respect to the applied EM field, can be considered as a complex scalar quantity [3]

$$\mu_{r,I} = \mu \pm \kappa \quad (5)$$

where μ and κ are the diagonal and off-diagonal components of the permeability tensor, respectively.

A positive (negative) sign in equation (5) corresponds to the clockwise (counter-clockwise) polarization of the magnetic field.

The permeability tensor components μ , κ and their sum exhibit resonance character. The FMR frequency f_{FMR} is defined as the frequency for which the denominator in expression (5) vanishes, which takes place when $f_{\text{FMR}} = \gamma H_0$ or $w = H_{0r}$.

2.3. Initial permeability

For ferromagnetic medium in the completely demagnetized state, the permeability tensor (2) becomes diagonal and is called the initial permeability. An initial permeability model has been developed by Schlömann [4] who assumed that material consists of a certain number of concentric oppositely magnetized cylindrical magnetic domains. Because the off-diagonal components of the permeability tensor in such a domain structure cancel out, the permeability tensor becomes diagonal when the volumes of the domains magnetized in the opposite directions become identical. Schlömann proved that for any symmetric, but otherwise arbitrary domain configuration the following relationship holds

$$\mu_{\text{eff}}^2 - \kappa_{\text{eff}}^2 = \mu^2 - \kappa^2. \quad (6)$$

Because the right-hand side of equation (6) does not depend on the domain configuration, the μ_{eff} considered as a function of the net magnetization approaches minimum when κ_{eff} vanishes. Taking into account (3) and (4), for lossless medium ($\alpha = 0$), the right-hand side of equation (6) can be written as

$$\mu_{\text{eff_min}}^2 = \frac{w^2 - (H_{\text{ar}} + 1)^2}{w^2 - H_{\text{ar}}^2}. \quad (7)$$

In the original paper [4] Schlömann assumed that in the completely demagnetized state the effective static magnetic field is equal to the anisotropy field so that in such a case $H_{\text{ar}} = H_a/M_s$. Formula (7) was derived under the assumption that in all the domains the magnetization vectors are parallel to the z -direction, so that $\mu_{\text{eff_min}}$ denotes the permeability component in the plane perpendicular to the z -axis. The permeability component along the z -axis for cylindrical domain configuration is equal to unity and it does not exhibit resonance character. The average initial permeability for randomly orientated domains is expected to be given as the average of the permeabilities along the three principal directions so the formula for the initial permeability can be written as follows [4]

$$\mu_d = \frac{2}{3} \left(\frac{w^2 - (H_{\text{ar}} + 1)^2}{w^2 - H_{\text{ar}}^2} \right)^{1/2} + \frac{1}{3}. \quad (8)$$

The minimum value of μ_d from equation (8) is equal to $1/3$. In real samples domain distribution is not random, but it depends on the shape of the sample. As will be shown later, experiments confirm the sample shape dependence of the initial permeability.

2.4. Anisotropy in single crystal samples

Single crystal ferromagnetic materials exhibit magnetic anisotropy which is related to their crystallographic structure. Magnetic anisotropy is usually described by anisotropy constants or, alternatively, by the anisotropy field. In cubic crystals, such as YIG, magnetic anisotropy is usually weak [3], while in hexagonal crystals, such as barium ferrite, it can be

very strong [5, 6]. As has been shown in [7], in the presence of small cubic anisotropy permeability and for arbitrary direction of the static magnetic field the permeability tensor takes the form (9)

$$\bar{\mu} = \mu_0 \begin{bmatrix} \mu_{11} & j\mu_{12} & j\mu_{13} \\ -j\mu_{12} & \mu_{22} & \mu_{23} \\ -j\mu_{13} & \mu_{23} & \mu_{||} \end{bmatrix}. \quad (9)$$

The components μ_{11} , μ_{12} and $\mu_{||}$ of tensor (9) are identical to the corresponding components of tensor (2). The additional tensor components μ_{13} and μ_{23} depend on the angle between the static internal magnetic field and the principal directions of the cubic cell.

As discussed earlier, the permeability tensor (2) becomes diagonal for a circularly polarized EM field in the plane perpendicular to the static magnetic field, but it is not generally true for the tensor given by (9). However, if the static magnetic field is applied along the hard axis of magnetization (one of the [100], [010] or [001] axes) or along the easy axis of magnetization (one of the [111] axes of the cubic crystal) the components μ_{23} and μ_{13} vanish and the tensor (9) becomes identical to (1).

The FMR frequency in the presence of anisotropy is different to that for isotropic materials and it depends on the orientation of \mathbf{H}_0 with respect to the principal crystal axes. As an example let us consider the case when \mathbf{H}_0 and \mathbf{M}_s are parallel, they are situated in the (100) plane of a cubic crystal and make the angle θ with the [001] axis of the crystal. Then the FMR frequency can be expressed as follows [3]:

$$f_{\text{FMR}} = \gamma \left(H_0 + H_a \left(-\frac{3}{8} + \frac{5}{2} \cos(2\theta) + \frac{15}{8} \cos(4\theta) \right) \right) \quad (10)$$

where: $H_a = 2 \frac{K_1}{M_s}$, K_1 is the first anisotropy constant, θ — the angle between the [001] axis and the \mathbf{H}_0 vector.

One notes that the maximum of the FMR frequency, $f_{\text{FMR_max}} = \gamma (H_0 + H_a)$, appears for $\theta = 0$. The minimum $f_{\text{FMR_min}} = \gamma (H_0 - \frac{2}{3} H_a)$ appears for $\theta = 54^\circ 44'$ (for the \mathbf{H}_0 vector which is parallel to one of the [111] crystal axes). The effective anisotropy field H_a in the single crystal YIG is approximately equal to 6.94 kA m^{-1} [3] for bulk samples and 6.6 kA m^{-1} for thin films [8]. Formula (10) is frequently used to determine the anisotropy field and the first anisotropy constants from measurements of the resonance frequencies versus the angle θ . More information on anisotropy in magnetic materials, particularly in thin films, can be found in [9].

For hexagonal ferrites the anisotropy field is very high leading to the FMR frequency at millimeter waves range. For $\text{BaFe}_{12}\text{O}_{19}$ $H_a = 1337 \text{ kA m}^{-1}$, while for $\text{Ba}_2\text{Co}_2\text{Fe}_{12}\text{O}_{22}$ $H_a = 2228 \text{ kA m}^{-1}$, which corresponds to the ferromagnetic frequency $f_{\text{FMR_max}}$ equal to 47 GHz for the first material and to 78 GHz for the second material without any external magnetic field bias. The saturation magnetization values for these materials are $M_s = 382 \text{ kA m}^{-1}$ for $\text{BaFe}_{12}\text{O}_{19}$ and $M_s = 183 \text{ kA m}^{-1}$ for $\text{Ba}_2\text{Co}_2\text{Fe}_{12}\text{O}_{22}$ [10, 11].

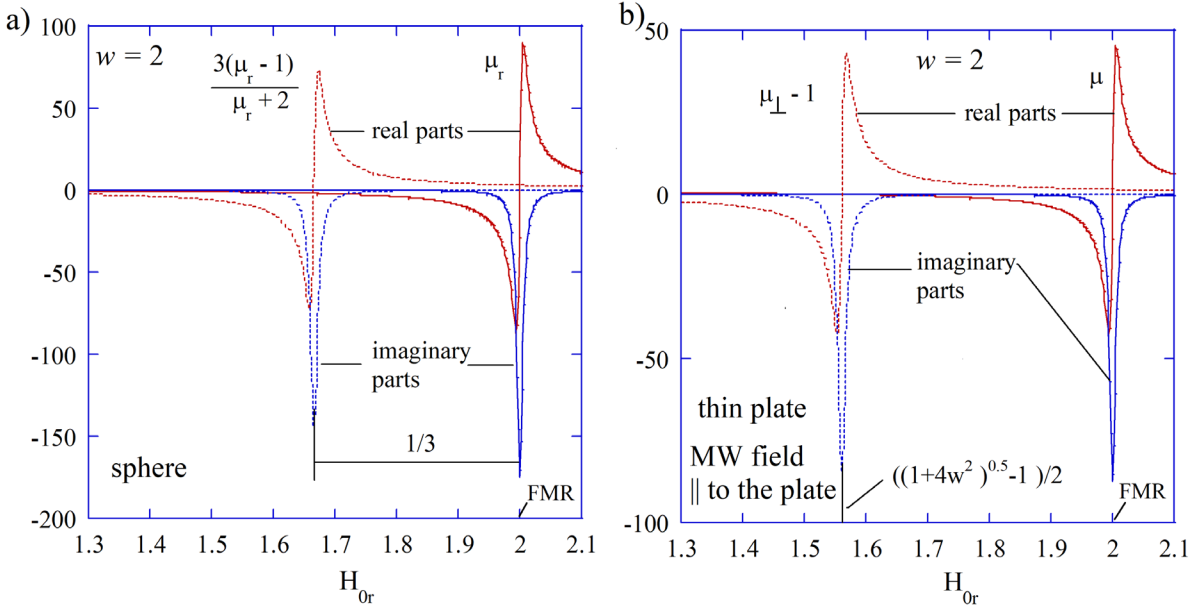


Figure 1. The intrinsic permeabilities and the external susceptibilities $F(\mu, \kappa, \mu_{||})$ versus normalized static magnetic field at the normalized frequency $w = 2$ assuming $\Delta H = 10$ Oe and $M_S = 140$ kA/m (a) for a spherical sample, (b) for a thin plate sample magnetized in its plane with the RF magnetic field which is tangential to the plate and orthogonal to the static magnetic field.

2.5. Relationship between the external and the internal static magnetic field in ferrite samples

Permeability tensor components depend on the internal static magnetic field in the sample so it is of practical interest to know the relationship between the static external and internal fields. The internal static magnetic field \mathbf{H}_0 in an ellipsoidal ferromagnetic sample, situated in a uniform static magnetic field \mathbf{H}_e , is uniform and it can be expressed by the well-known formula $\mathbf{H}_0 = \mathbf{H}_e - \bar{N}\mathbf{M}_S$ where \bar{N} denotes the demagnetization tensor. The eigenvalues of this tensor are called demagnetization factors and they are tabulated for ellipsoidal samples [12]. The sum of demagnetization factors is equal to unity. All three demagnetizing factors for a spherical sample are equal to 1/3. Often demagnetizing factors of degenerate forms of ellipsoid (thin disc, long cylinder) are used to determine the internal field in such samples. However, in cylindrical samples, that are commonly used in the magnetic measurements, the demagnetizing field $\mathbf{H}_d = \bar{N}\mathbf{M}_S$ is not uniform, therefore, two kinds of static permittivity-dependent demagnetizing factors are defined for cylindrical samples. The fluxmetric demagnetizing factor N_f is defined as the ratio of the average demagnetizing field to the average magnetization at the midplane perpendicular to the axis. The magnetometric demagnetizing factor N is defined as the ratio of the average demagnetizing field to the average magnetization of the entire sample. Demagnetizing factors (both fluxmetric and magnetometric) for cylindrical samples with different aspect ratios and different static permeabilities are tabulated in [13].

2.6. Perturbation theory and the external susceptibilities

Perturbation theory is one of the most frequently used methods for determination of the resonance frequency and Q -factor changes of resonators containing gyromagnetic samples. In

perturbation theory the relationship between the complex frequency of an empty cavity and the complex frequency of the cavity containing the ferromagnetic sample is expressed as follows

$$\frac{\hat{f} - \hat{f}_0}{\hat{f}} = -C_1 F(\mu, \kappa, \mu_{||}) - C_2 G(\varepsilon_f) \quad (11)$$

where: $\hat{f}_0 = f'_0 + j\frac{f'_0}{2Q_0}$, $\hat{f} = f' + j\frac{f'}{2Q}$ denote complex frequencies of the empty and perturbed cavity, respectively, Q_0 and Q represent the corresponding unloaded Q -factors, C_1 and C_2 are perturbation constants that are of the order of V_s/V_0 , where V_s and V_0 denote the volume of the sample and the cavity, respectively.

Functions $F(\mu, \kappa, \mu_{||})$ and $G(\varepsilon_f)$ depend on the shape of the sample being tested and its position in the cavity. Perturbation expressions can be found in several papers and books [3, 14]. They were derived for spheroidal shape samples situated in a uniform microwave magnetic field under quasi-magnetostatic approximation and they are used for spherical, thin cylindrical rod and thin disc samples being the degenerate forms of spheroid. The most frequently used magnetic perturbation functions $F(\mu, \kappa, \mu_{||})$ are: $F = 3(\mu \pm \kappa - 1)/(\mu \pm \kappa + 2)$ for a spherical sample situated in a circularly polarized magnetic field; $F = 2(\mu \pm \kappa - 1)/(\mu \pm \kappa + 1)$ for thin, a cylindrical rod situated in a circularly polarized magnetic field; $F = (\mu - 1)/\mu$ for a thin plate magnetized in its plane situated in the RF magnetic field normal to the plate; and $F = \mu_{\perp} - 1$, for a thin plate magnetized in its plane situated in the RF magnetic field tangential to the plate and orthogonal to the DC magnetic field. Functions $F(\mu, \kappa, \mu_{||})$ are often referred to as the external susceptibilities of the samples [15]. It should be emphasized that the external susceptibilities do not describe the intrinsic properties of gyromagnetic material, but they are formally analytic functions of a complex variable.

The relationship between the internal permeability and the external susceptibility can be considered as a conformal mapping. In figure 1 the internal and the external permeabilities are plotted for spherical and thin plate samples.

As shown in figure 1, plots of the external and internal permeability versus the static magnetic field look similar but they are shifted on the abscissa axis. The condition for the FMR (Polder resonance) does not depend on the shape of the sample and it is given by the expression $w = H_{0r}$. Resonances of the external susceptibilities (Kittel's resonances [16]) depend on the shape of the samples. Kittel's resonance conditions for the cases presented in figure 1 are: $w = H_{0r} + 1/3$ for a spherical sample and $w = (H_{0r}(H_{0r} + 1))^{0.5}$ for a thin plate sample. One can see that the effective internal permeability values at Kittel's resonance for lossless gyromagnetic material are as follows: $\mu_r = \mu + \kappa = -2$ for a spherical sample, $\mu_r = \mu + \kappa = -1$ for a cylindrical rod sample and $\mu = 0$ for thin plate samples. These effective permeability values can be derived from equations (3) and (4) assuming $\alpha = 0$. In the majority of measurement techniques of permeability tensor perturbation theory has been employed. Two permeability tensor components μ and κ were determined from measurements of the resonance frequencies and Q -factors of two oppositely polarized modes. Oppositely polarized TM_{110}^+ and TM_{110}^- modes of a cylindrical cavity have been used most frequently, but another pair of circularly polarized modes can also be employed. One should note that at FMR the values of functions F (the external permeability) converge to a constant value and their values would be very similar for large internal permeabilities (e.g. for a spherical sample and $\mu_r = \mu + \kappa = \infty$, $F(\mu_r) = 3$ and for $\mu_r = 100$, $F(\mu_r) = 2.94$). For this reason, determination of the internal permeability from the measured external permeability, as $\mu_r = F^{-1}$ (at FMR), is rather inaccurate: particularly for narrow FMR linewidth materials, when the internal permeability values can be as large as a few thousand. Researchers usually measure resonance phenomena in ferromagnetic materials near resonances of the external permeability. This is justified because the graphs of the internal and external permeabilities look very similar to each other. However, it should be emphasized that the internal permeability values determined from such experiments are small and they are situated on the tails of resonances of the internal permeability tensor components. It should also be pointed out that the perturbation theory fails when samples are large or even if samples are small but are made of narrow linewidth materials, such as monocrystalline YIG.

3. Rigorous electrodynamic approach—transcendental equations

Formally, free oscillations of a resonance structure can be formulated by using a boundary value problem for Maxwell's equations. The eigenvalues of this problem describe free oscillations of a resonance system surrounded by a perfectly conducting enclosure and denote the complex eigenfrequencies $\hat{\omega}_s = \omega'_s + j\omega''_s$ of specific modes. The Q -factors due to dielectric and magnetic losses of these modes can be computed

as $Q_s = \omega'_s / (2\omega''_s)$. Rigorous solutions of Maxwell's equations for resonators containing gyromagnetic samples are available for a few simple geometries where permeability and permittivity vary only along one axis of rectangular, cylindrical or spherical coordinate systems that are depicted in figure 2.

Two kinds of resonances should be distinguished. The first are resonances of ferromagnetic samples in free space (figure 2(f)) and the second are resonances in shielded structures where the sample is situated either in a closed metal cavity or it is partly shielded by metal walls to prevent radiation, e.g. in the structures shown in figures 2(b) and (c).

Resonance frequencies of isolated gyromagnetic spheroids were studied, for the first time, by Walker [17] in 1958. He derived a transcendental equation (TDE) that allowed him to determine the relationship between the normalized resonance frequency and the normalized internal magnetic field of an isolated gyromagnetic spheroid. The TDE was derived by Walker under the assumption that the microwave magnetic field in a gyromagnetic spheroid, magnetized along the axis of its revolution, satisfies equations $\text{div}\mathbf{B} = 0$ and $\text{curl}\mathbf{H} = 0$, that are equations of the magnetostatic. Further, Fletcher and Bell presented specific solutions of Walker's TDE for a gyromagnetic sphere [18]. The magnetostatic TDE is also known for a cylindrical rod sample situated between two infinite parallel conducting planes [19]. Solutions of the TDEs introduced by these researchers are known as quasi-magnetostatic (QMS) modes; although this is a misleading name because resonances appear at microwave frequencies. The eigenvalues of the QMS-TDEs correctly determine the relationship between the normalized resonance frequencies and the normalized static magnetic field for small samples with dimensions that are much smaller than the wavelength. For historical reasons, the majority of researchers call the free oscillations in isolated gyromagnetic objects (usually spheroids and their degenerate forms) free oscillations of the magnetostatic modes.

For the resonance structures shown in figure 2 the relationship between the complex resonance frequency and the material properties (permittivity, permeability tensor components) can be formulated as a TDE. Derivations of TDEs can be found in several papers and textbooks. Although some of these equations have been known for decades, they are not frequently used in practice. In the past this has been justified because of the lack of computational resources, but these days solving a TDE is a typical, although nontrivial, task of numerical techniques. It should be pointed out that, so far, there are only a few papers that describe the solutions of TDEs in their most general form when the complex permeability components are dispersive and lossy. A TDE for all modes of gyromagnetic cylindrical rod (figure 2(b)) was derived in [20] by Godtmann and Haas. Derivation was based on the earlier works published by Kales [21] and Epstein [22], and is also presented in Gurevich's textbook [3]. An extension of the Godtmann and Haas equation to the multilayer structure shown in figure 2(c) was employed by Krupka [23] in measurements of all permeability tensor components of ferrite rods. Derivation of the TDE for the TM_{mn0} modes in a rectangular cavity shown in

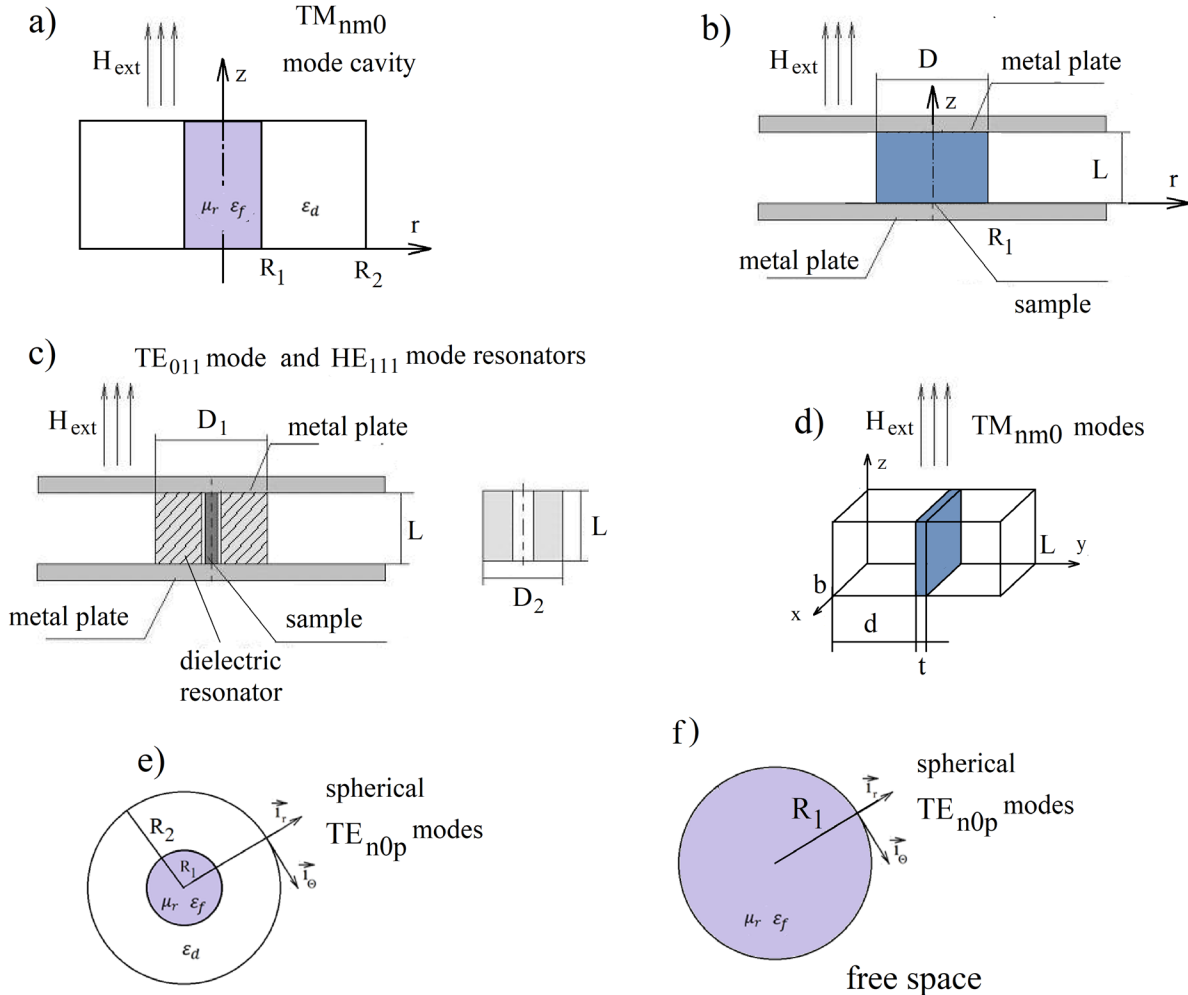


Figure 2. Resonance systems containing gyromagnetic samples for which rigorous solutions of Maxwell's equations are available. (a) Cylindrical cavity containing cylindrical rod sample. (b) Cylindrical rod sample between two infinite conducting planes. (c) Rod sample in cylindrical dielectric resonator between two infinite conducting planes. (d) Rectangular cavity with slab sample fully occupying its cross-section. (e) Spherical sample situated in spherical cavity. (f) Spherical sample in free space.

figure 2(d) can be found in [3]. To be more precise, the equation in [3] was derived for a rectangular waveguide containing ferrite slabs. One of the most frequently used resonance structures for measurements of permittivity and permeability tensor components of rod shape samples is the cylindrical TM_{nm0} mode cavity shown in figure 2(a). The appropriate TDE for this structure was presented by Bussey [24], and its derivation can also be found in [25, 26]. Finally, TDEs for the TE_{n0p} modes of a spherical cavity containing spherical gyromagnetic samples and spherical gyromagnetic samples in free space figure 2(f), and in a spherical metal cavity figure 2(e) are presented in [27, 28]. Below we present some of these TDEs that will be solved or referred to in the following sections of this paper.

The TDE for the TE_{n0p} mode in a gyromagnetic sphere magnetized perpendicularly to the $\mathbf{i}_r, \mathbf{i}_\theta$ plane (figure 2(f)) can be written as follows [27]

$$\left\{ n J_{n+\frac{1}{2}}(kR_1) - k J_{n-\frac{1}{2}}(kR_1) \right\} H_{n+\frac{1}{2}}^{(2)}(k_0 R_1) - \mu_r \left\{ n H_{n+\frac{1}{2}}^{(2)}(k_0 R_1) - k_0 H_{n-\frac{1}{2}}^{(2)}(k_0 R_1) \right\} J_{n+\frac{1}{2}}(kR_1) = 0 \quad (12)$$

where $k = \hat{\omega}/c(\epsilon_f \mu_r)^{0.5}$, $k_0 = \hat{\omega}/c(\epsilon_d)^{0.5}$, $\hat{\omega} = \omega' + j\omega'' = 2\pi f$. ϵ_f (ϵ_d) is the relative complex permittivity of the sphere (the medium surrounding the sphere) and μ_r is the relative complex permeability of the sphere (5). In equation (12) n , p denote elevation and radial mode indices, respectively, c is the speed of the EM wave in a vacuum and $J(H)$ are Bessel (Hankel) functions.

It should be emphasized that the angular frequency should be complex not only in equation (12), but also in the definitions of the permeability tensor components.

The TDE for the TM_{mn0} modes of the cylindrical cavity shown in figure 2(a) is given by (13) [23].

$$\frac{k_1 R_1 J'_n(k_1 R_1)}{\mu_\perp J_n(k_1 R_1)} \mp n K = \frac{k_1 R_1 C'_n(k_2 R_1)}{C_n(k_2 R_1)} \quad (13)$$

where:

$$C_n(k_2 r) = J_n(k_2 r) - Y_n(k_2 r) J_n(k_2 R_2) / Y_n(k_2 R_2)$$

$$k_1 = \frac{\hat{\omega}}{c} (\epsilon_f \mu_\perp)^{0.5}, k_2 = \frac{\hat{\omega}}{c} (\epsilon_d)^{0.5}$$

$$\mu_{\perp} = \frac{\mu^2 - \kappa^2}{\mu}, K = \frac{-\kappa}{\mu^2 - \kappa^2}$$

where Y is the Bessel function of the second kind.

The symbol prime denotes the derivative with respect to the argument.

The TDE for the TM_{mn0} modes of the rectangular cavity shown in figure 2(a) is given by (13) [3].

$$\det \begin{bmatrix} S_1 & 0 & -1 & 0 \\ p_0 C_3 & -p & q & 0 \\ 0 & S_2 & C_2 & -S_4 \\ 0 & qS_2 - pC_2 & qC_2 + pS_2 & -p_0 C_4 \end{bmatrix} = 0 \quad (14)$$

$$S_1 = \sin(k_2 d), C_3 = \cos(k_2 d), S_2 = \sin(k_1 t), C_2 = \cos(k_1 t),$$

$$S_4 = \sin(k_2(L - d - t)), C_4 = \cos(k_2(L - d - t)),$$

$$k_1 = \left[\left(\frac{\hat{\omega}}{c} \right)^2 \varepsilon_f \mu_{\perp} - \left(\frac{n\pi}{b} \right)^2 \right]^{0.5}$$

$$k_2 = \left[\left(\frac{\hat{\omega}}{c} \right)^2 - \left(\frac{n\pi}{b} \right)^2 \right]^{0.5}$$

$$\varepsilon_f = \varepsilon'_f - j \frac{\sigma}{\omega \varepsilon_0}$$

$$p_0 = k_2,$$

$$p = k_1 / \mu_{\perp}$$

$$q = \frac{n\pi}{b} \frac{\kappa}{\mu \mu_{\perp}}$$

where σ is the conductivity (S m^{-1}) and ε_0 is the permittivity of the vacuum.

One widely cited TDE presented by Courtney [29] should be mentioned. From a theoretical point of view, it is only a special case of the Godtmann and Haas equation for the TE_{0np} modes of a cylindrical isotropic rod presented in figure 2(b). On the other hand, it has been so widely cited because it creates a theoretical background for one of the most accurate methods of the complex permittivity and the complex initial permeability measurements of low loss microwave garnets and ferrites. Courtney's equation can be written as

$$\mu_d k_2 J_1(k_1 R_1) K_0(k_2 R_1) + k_1 J_0(k_1 R_1) K_1(k_2 R_1) = 0. \quad (15)$$

Where: $k_1 = \left(\left(\frac{\omega}{c} \right)^2 \varepsilon_f \mu_d - \left(\frac{p\pi}{L} \right)^2 \right)^{0.5}$, $k_2 = \left(\left(\frac{p\pi}{L} \right)^2 - \left(\frac{\omega}{c} \right)^2 \right)^{0.5}$ and K_n denotes modified Bessel functions.

The Q_s -factor evaluated from solutions of TDE's as $Q_s = \omega_s' / (2\omega_s'')$ depends on the sum of the dielectric and the magnetic losses inside the resonator. Formally, Q_s can be separated into the parts depending on the dielectric and the magnetic losses as $Q_s = 1 / (1/Q_d + 1/Q_m)$. The measured unloaded Q -factor of the resonator also includes conductor

losses in metal cavity walls (or in the metal shield) according to the formula $Q = 1 / (1/Q_s + 1/Q_c)$, where Q_c is the Q -factor due to conductor losses.

It is often assumed that for small samples $Q_c = Q_0$ (Q_0 is the Q -factor of the empty cavity) but at frequencies that are close to the magnetic plasmon or another spin wave resonance the Q -factor due to conductor losses can be substantially larger than Q_0 . This has been shown for small gyromagnetic spherical samples situated in a large spherical cavity [28].

TDEs create a theoretical background for rigorous and the most accurate methods of permittivity, permeability and ferromagnetic linewidth measurements and they deserve to be used more frequently in practice. Free MATLAB programs for solving magnetostatic TDEs for spheres and cylindrical rods and magnetodynamic TDEs for some modes of the structure shown in figure 2(c) and a gyromagnetic sphere can be found at <http://ztm.ire.pw.edu.pl/aktywnosc/projekty-badawcze/projekt-team-tech-en/>.

Readers who are not familiar with rigorous methods for the solution of boundary value problems for transmission lines and resonators containing gyromagnetic media are referred to the basic literature on this topic, e.g. [3] where these problems are discussed in detail.

3.1. Theoretical analysis of the resonance frequencies and Q -factors employing an electrodynamic approach

In this section results of theoretical computations of the normalized resonance frequencies and Q -factors due to dielectric and magnetic losses are presented. As the first example we solved the TDE (13) for TM_{110}^{\pm} modes of a cylindrical cavity and ferrite sample for which the measurement results were published [30]. Results of the computations of the normalized resonance frequencies versus the normalized internal static magnetic field are presented in figure 3. It is seen that apart from the dominant magnon–polariton modes (figure 3(a)) that are employed in the determination of μ and κ , manifolds of spin wave modes are present on the right-hand side of the asymptotic line $w = \sqrt{H_{0r}(H_{0r} + 1)}$ corresponding to $\mu = 0$. It should be noted that there are infinite numbers of modes in the vicinity of $\mu = 0_-$ in the two manifolds for both the clockwise TM_{110}^+ and the counter-clockwise TM_{110}^- polarizations. Physically it is understood because the radial propagation constant in the sample $k_1 = \frac{\omega}{c} (\varepsilon_f \mu_{\perp})^{0.5}$ converges to infinity when μ converges to 0_- . Formally, the spin modes belonging to the two manifolds should be named as the quasi TM_{1n0}^+ and the quasi TM_{1n0}^- modes.

In figure 4 results of the computations of the normalized resonance frequencies of the TM_{010} of a cylindrical resonator which is used in our experiments versus a normalized internal static magnetic field are presented. For this mode, in the absence of a gyromagnetic sample, only the axial component of the electric field and the azimuthal component of the magnetic field are present. As for the TM_{110}^{\pm} mode resonator, and also for the TM_{010} resonator, apart from the dominant magnon–polariton mode of the cavity, a manifold of spin wave modes is present on the right-hand

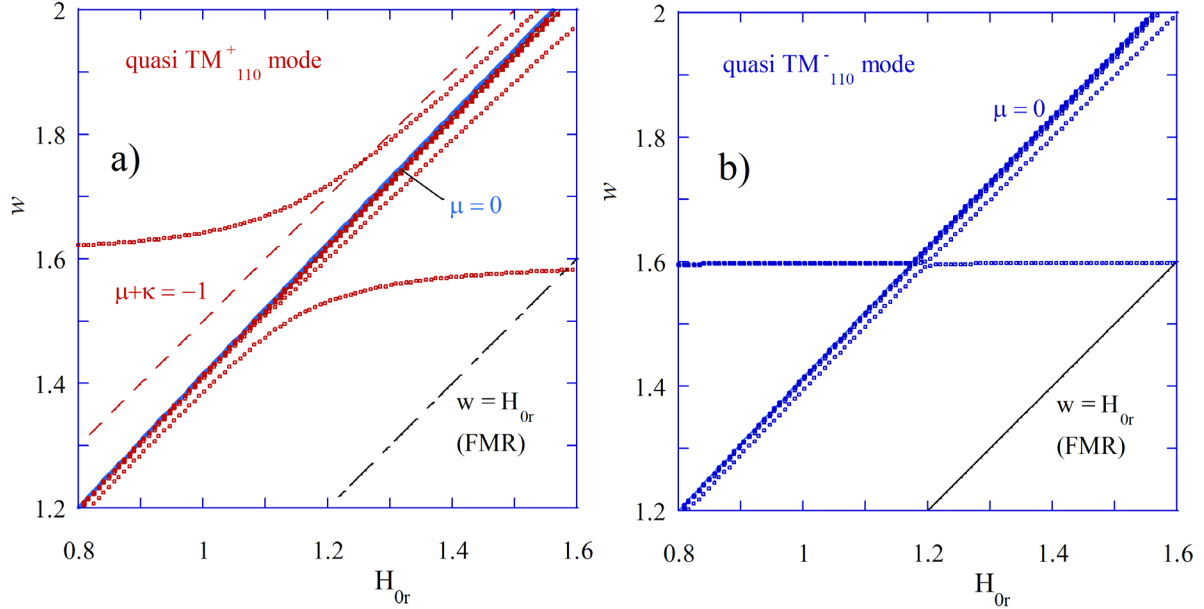


Figure 3. Computed normalized quasi TM_{110}^\pm mode resonance frequencies versus normalized internal static magnetic field bias for a cylindrical cavity with the TM_{110} mode resonance frequency, while empty, $f_0 = 9860$ MHz ($R_2 = 18.542$ mm), containing a ferrite sample with radius $R_1 = 1.0$ mm, $M_S = 175$ kA m $^{-1}$, $\epsilon_f = 12.5$, $\Delta H = 0.5$ Oe. Measurement results in [30] were presented for $H_{0r} > 1.35$ and for $H_{0r} < 0.8$.

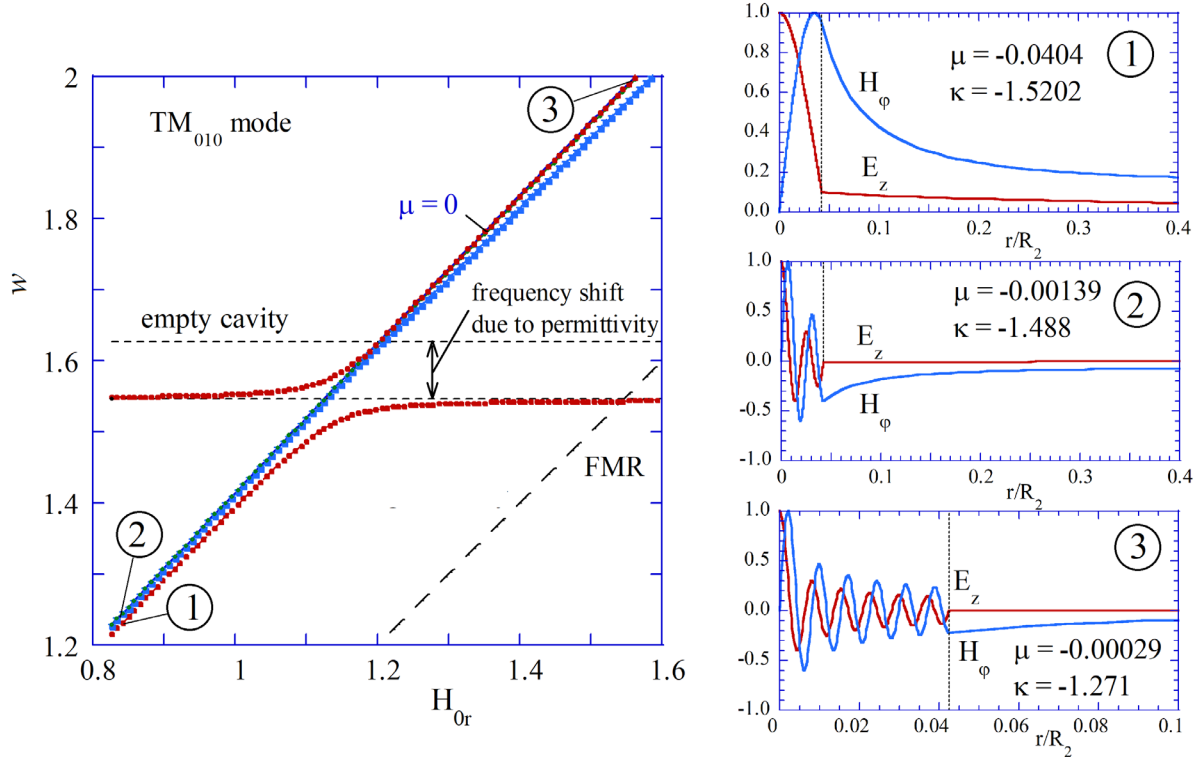


Figure 4. (a) Computed normalized quasi TM_{010} mode resonance frequencies versus normalized internal static magnetic field bias for a cylindrical cavity with the TM_{010} mode resonance frequency, while empty, $f_0 = 2458$ MHz ($R_2 = 46.67$ mm), containing a ferrite sample with radius $R_1 = 1.98$ mm, $\epsilon_f = 14.3$, $M_S = 43$ kA m $^{-1}$, (b) electric and magnetic field distributions for three different spin wave TM_{0n0} modes marked in the figure on the left.

side of the asymptotic line $w = \sqrt{H_{0r}(H_{0r} + 1)}$ corresponding to $\mu = 0$. In the three subplots of figure 4 the electric and magnetic field distributions are shown for different modes belonging to the spin wave manifold. In the subplots it is seen that the $e\text{-}m$ fields outside the sample

exhibit evanescent character. Propagation constants in the sample k_1 for these modes are very large, similar to those for the TM_{110}^\pm modes. Formally, all the modes belonging to the manifold should be named as quasi TM_{0n0} modes. Results of the computations shown in figures 3 and 4 were obtained

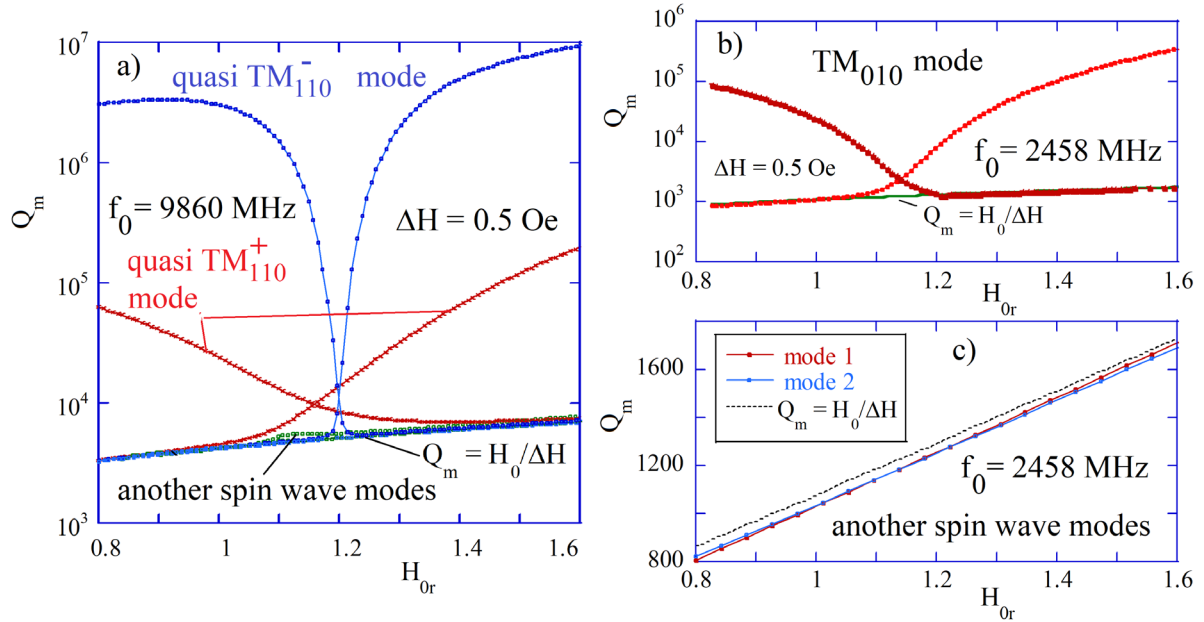


Figure 5. (a) Computed Q -factors due to magnetic losses Q_m of quasi TM_{1n0}^\pm modes versus normalized internal static magnetic field bias for a cylindrical cavity with the TM_{110} mode resonance frequency $f_0 = 9860$ MHz ($R_2 = 18.542$ mm), containing a ferrite sample with radius $R_1 = 1.0$ mm, $M_S = 175$ kA m $^{-1}$, $\epsilon_f = 12.5$, $\Delta H = 0.5$ Oe. (b) Computed Q -factors due to magnetic losses Q_m of quasi TM_{0n0} modes versus normalized internal static magnetic field bias for a cylindrical cavity with the TM_{010} mode resonance frequency $f_0 = 2458$ MHz ($R_2 = 46.67$ mm), containing a ferrite sample with radius $R_1 = 1.98$ mm, $M_S = 43$ kA m $^{-1}$, $\epsilon_f = 14.3$, $\Delta H = 0.5$ Oe. (c) The computed Q_m of quasi TM_{010} and quasi TM_{030} modes employing formula (16).

for lossless samples. When the linewidth of a gyromagnetic sample increases the losses would have an influence on the resonance frequencies. By solving the TDE for $\Delta H > 0$ one can find the complex eigenfrequencies $\hat{\omega}_s = \omega'_s + j\omega''_s$, belonging to a specific mode family, and the corresponding Q -factors due to dielectric and magnetic losses of these modes as $Q_s = \omega'_s / (\omega''_s)$.

The results of the computations of the Q -factors due to magnetic losses (Q_m) for TM_{1n0}^\pm and TM_{0n0} modes of the same resonators that were analyzed in figures 3 and 4, are presented in figure 5, assuming $\Delta H = 0.5$ Oe. At the frequency ranges where the mode spectrum is dense (near the asymptote $\mu = 0$) it is very difficult to determine the Q -factors of different modes by solving the TDE with respect to the complex frequency. As shown in [27], the Q -factor of the s th mode of free oscillations of the resonator containing dispersive media can be alternatively determined from the following formula:

$$Q_s = \frac{\frac{1}{4} \left\{ \iiint_V \frac{\partial[\omega'_s \epsilon'_a(\omega'_s)]}{\partial \omega} |\mathbf{E}_s|^2 dv + \iiint_V \frac{\partial[\omega'_s \mu'_a(\omega'_s)]}{\partial \omega} |\mathbf{H}_s|^2 dv \right\}}{\frac{1}{2} \left(\iiint_V \epsilon''_a(\omega'_s) |\mathbf{E}_s|^2 dv + \iiint_V \mu''_a(\omega'_s) |\mathbf{H}_s|^2 dv \right)} \quad (16)$$

where $\epsilon_a = \epsilon'_a - j\epsilon''_a$ ($\mu_a = \mu'_a - j\mu''_a$) is the absolute complex permittivity (permeability) inside the resonator.

The denominator in equation (16) denotes the average total energy dissipated in the resonator (P_{loss}), while the numerator can be interpreted as the average total EM energy stored in the resonator. A similar expression for the total EM energy stored in dispersive media can be found in [31–36]. For the TM_{mn0} modes, μ_\perp represents the effective permeability of a gyromagnetic medium, and if the dielectric losses are negligible one can rewrite (16) as:

$$Q_s = \frac{\frac{1}{4} \left\{ \iiint_V \frac{\partial(\omega \mu'_\perp)}{\partial \omega} |\mathbf{H}|^2 dv + \iiint_V |\mathbf{E}|^2 dv \right\}}{\frac{1}{2} \iiint_V \mu''_\perp |\mathbf{H}|^2 dv}. \quad (17)$$

Assuming $\alpha = 0$ in the permeability tensor components given by expressions (2) and (3) one can obtain an analytic formula for $\partial(\omega \mu'_\perp) / \partial \omega$ as follows

$$\begin{aligned} \frac{\partial(\omega \mu'_\perp)}{\partial \omega} &= \mu'_\perp + w \frac{\partial(\mu'_\perp)}{\partial \omega}, \frac{\partial(\mu'_\perp)}{\partial \omega} \\ &= \left[1 + \left(\frac{\kappa'}{\mu'} \right)^2 \right] \frac{\partial(\mu')}{\partial w} - \frac{2\kappa'}{\mu'} \frac{\partial(\kappa')}{\partial w}. \end{aligned}$$

When the electromagnetic field distribution in the cavity containing a gyromagnetic sample is known, the Q -factor due to conductor losses, Q_c , can be rigorously evaluated from the formula

$$Q_c = \omega'_s \frac{\frac{1}{4} \left\{ \iiint_V \frac{\partial[\omega'_s \epsilon'_a(\omega'_s)]}{\partial \omega} |\mathbf{E}_s|^2 dv + \iiint_V \frac{\partial[\omega'_s \mu'_a(\omega'_s)]}{\partial \omega} |\mathbf{H}_s|^2 dv \right\}}{\frac{1}{2} R_S \left(\iint_S |\mathbf{H}_\tau|^2 ds \right)} = \frac{G}{R_S} \quad (18)$$

where: R_S is the surface resistance of the metal cavity walls (Ω), G is the geometric factor (Ω), S is the surface of the cavity, and \mathbf{H}_τ is the magnetic field component tangential to the walls of the cavity.

Computations of the Q -factors due to magnetic losses from formulae (17) for the first two spin wave modes are shown in figure 5(c). It is seen that the computed Q -factor results are close to the value $Q_m = H_0 / \Delta H$. Similar Q -factor values for these modes were obtained from the solution of a TDE as shown in figure 5(b). Important physical conclusions can be

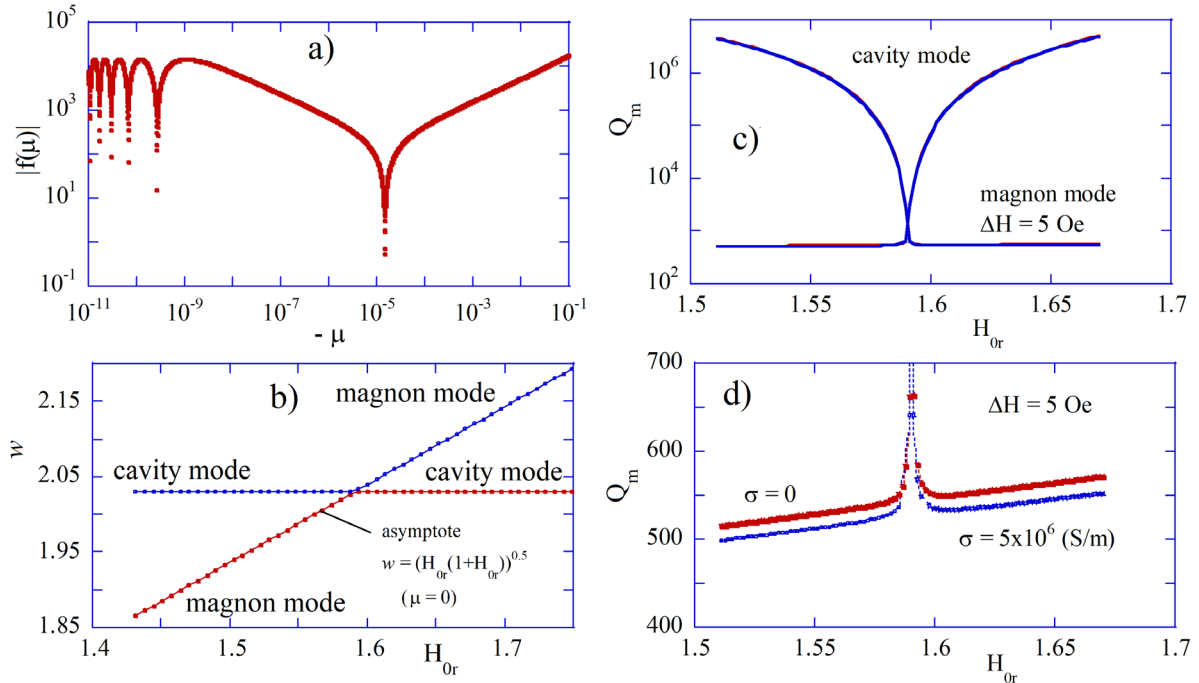


Figure 6. (a) The modulus of determinant as a function of the diagonal component of a permeability tensor. Minima in this graph correspond to the subsequent roots of a TDE (ordered from the right to the left), (b) normalized resonance frequencies versus a normalized internal static magnetic field, (c) and (d) Q -factors due to magnetic and dielectric losses in a thin gyromagnetic sample. Computations have been performed for: $L = 2b$, $d = (L - t)/2$ (sample at the center of the cavity at minimum electric field), $t = 50$ nm, the TM_{120} mode resonance frequency $f_0 = 10$ GHz, $M_S = 140$ kA m $^{-1}$, $\Delta H = 5$ Oe.

drawn from analysis of the $\partial(\omega\mu'_\perp)/\partial\omega$ values. The higher the mode number (the mode which is situated closer to the asymptote $\mu = 0$), the larger these values are. For the TM_{030} mode and $H_{0r} = 0.8$ the value is $\frac{\partial(\omega\mu'_\perp)}{\partial\omega} > 10^5$. This means that the magnetic energy stored in the gyromagnetic medium $W_m = \frac{1}{4} \iiint_V \frac{\partial(\omega\mu'_\perp)}{\partial\omega} |\mathbf{H}|^2 dv$ also becomes very large, so that even if the μ''_\perp value in this case is in the order of a few hundred, the ratio of the stored to the dissipated energy, and therefore also the Q -factor, are in the order of 1000. It is important to note that the lower limit of the Q -factors due to magnetic losses for all modes is practically the same: $Q_m \approx H_0/\Delta H$. It should also be noted that the resonance frequency and the Q -factor curves versus H_{0r} in the vicinity of the FMR are smooth, so that FMR is not directly observed; however, μ and κ can be determined from these smooth measurement data and they exhibit resonance character. As shown in figures 3 and 4, the resonance frequencies for the TM_{010} and the TM_{110}^+ magnon-polariton modes converge to the asymptotic line $w = \sqrt{H_{0r}(H_{0r} + 1)}$.

As has been shown in [37] the normalized resonance frequencies of the HE_{111}^+ magnon-polariton mode for the resonance structure shown in figure 2(c) converge to the asymptotic line corresponding to the magnetic plasmon resonance (MPR) for a cylindrical sample $w = H_{0r} + 1/2$ which is equivalent to ($\mu + \kappa = -1$), while other modes belonging to the spin wave manifold converge to the asymptotic line $w = \sqrt{H_{0r}(H_{0r} + 1)}$.

In figure 6 the results of computations of the normalized resonance frequencies and Q -factor due to magnetic and

conductor losses in a thin ($t = 50$ nm) gyromagnetic sample are presented for the quasi TM_{110} mode for which the electric field at the center of the sample vanishes. Computations were performed as follows. As the first step for a given H_{0r} a TDE (14) was solved for lossless media with respect to the inverse of the diagonal component of the permeability tensor. For $\alpha = 0$, w and κ can be expressed through μ and H_{0r} according to (3) and (4). A graph of the modulus of the determinant (14) versus $-\mu$ is shown in figure 6(a). The root (minimum) near $|\mu| \approx 10^{-5}$ corresponds to the quasi-uniform magnetic field distribution in the sample. The subsequent roots correspond to higher order modes for which $k_1 t \approx m\pi/2$. One can note that theoretically (for the lossless sample) there is an infinite number of modes as $-\mu$ approaches 0. When the sample is thin the resonance frequencies for the subsequent modes practically overlap on the frequency scale and they are situated near the asymptotic line $w = \sqrt{H_{0r}(H_{0r} + 1)}$, as shown in figure 6(b). When the real TDE is solved the normalized real frequency w is then known and this sets the starting point for solving the complex TDE (14) with respect to the complex normalized frequency \hat{w} . For a thin sample and finite losses due to mode overlapping only one complex root (\hat{w}) can be determined. The real part of \hat{w} is practically the same as the w value for the first mode in the lossless case.

In figures 6(c) and (d) Q -factor values due to magnetic and dielectric losses being the solutions to the complex TDE are shown as functions of H_{0r} for the following parameters of the cavity and the sample: $L = 2b$, $d = (L - t)/2$ (the sample at the center of the cavity), $t = 50$ nm, the TM_{210} mode resonance frequency $f_0 = 10$ GHz, $M_S = 140$ kA m $^{-1}$, $\Delta H = 5$ Oe.

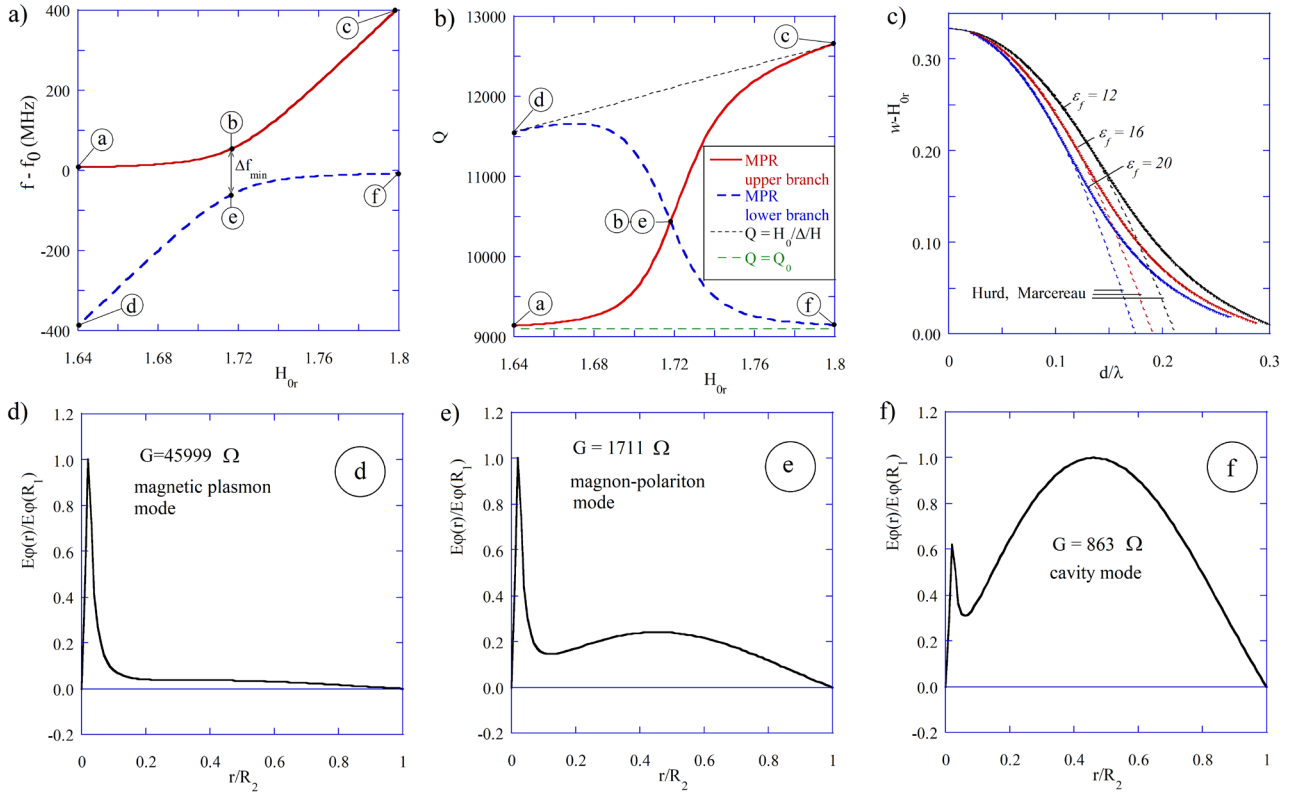


Figure 7. (a) Resonance frequency shifts $f - f_0$ and (b) the total unloaded Q -factors for a spherical TE_{101}^+ mode cavity having $f_0 = 10$ GHz ($R_2 \approx 21.3$ mm) containing a narrow linewidth spherical ferromagnetic sample with $R_1 = 0.5$ mm, $M_S = 140$ kA m $^{-1}$ and $\Delta H = 0.25$ Oe, (c) changes in the TE_{101}^+ mode resonance condition ($w - H_{0r}$) for a spherical sample in free space as a function of the relative diameter of the sample, d —diameter of the sample, $\lambda = c/f$. (d)–(f) Electric field distributions at the points marked with letters from (d)–(f) in figure 3(a). © Reproduced from [28]. © IOP Publishing Ltd. All rights reserved.

The results of the computations are shown for a dielectrically lossless sample having $\epsilon_f = 16$ and for a strongly conducting sample ($\sigma = 5 \times 10^6$), which corresponds to the complex permittivity $\epsilon_f \approx 16 - j \times 10^7$ at 10 GHz ($\epsilon_f = 16 - j \frac{\sigma}{\omega \epsilon_0}$). Such conductivity is similar to the conductivity of Permalloy or Heusler alloys. The lower Q -factor limit for the dielectrically lossless sample is very close to the line $Q_m = \frac{H_0}{\Delta H}$, which is similar to that for cylindrical rod samples in cylindrical cavities shown in figure 5. As shown in 6d, conductor losses reduce the Q_m -factor and thus the effective ΔH by about 4% which is noticeable but is a relatively small effect when taking into account the extremely large value of conductivity. It should be noted that the influence of dielectric losses is so small because the thin sample is situated in the cavity at the minimum of the electric field. If the sample is moved away from this position, Q -factor changes due to finite conductivity of the sample would be significant. The most important observation for a thin sample is that the dominant part of the total magnetic energy in the cavity is concentrated in the sample. Thus, the thin film itself creates itself a ‘spin resonator’ or magnon, similar to a thin rod sample in a cylindrical cavity (figures 4 and 5).

In figure 7 the results of the computations of the TE_{101}^+ mode resonance frequencies, Q -factors, resonance conditions and the electric field distributions are shown for a small spherical sample situated in a spherical cavity (figure 2(e)) (after

[28]). For small samples, the normalized resonance frequencies of the TE_{101}^+ magnon–polariton mode for the resonance structure converge to the asymptotic line corresponding to the MPR, which is also named as the mode of uniform precession in the magnetostatic approximation. The condition for this resonance for a small spherical sample in free space is $w = H_{0r} + 1/3$, which is equivalent to $(\mu + \kappa = -2)$. Similar to cylindrical and thin slab samples, Q -factors for MPR modes converge to the asymptotic value $Q_m = H_0/\Delta H$ (points c and d in figures 7(a) and (b)). For the assumed value of $\Delta H = 0.25$ Oe, Q_m values are in the range 11 500–12 700 at 10 GHz. When the resonance frequencies converge to the frequency of the empty cavity the total Q -factor (including the Q -factor due to conductor losses in metal cavity walls) then converges to the Q -factor of the empty cavity (points a and f in figures 7(a) and (b)). The Q -factor of the empty cavity was assumed to be 9100.

It should be noted that for the empty spherical TE_{101} mode cavity $G = G_0 = 846 \Omega$ (figure 7(f)), but at MPR the geometric factor G increases about 50 times (figure 7(d)); therefore, the Q -factor due to conductor losses Q_c also increases by a factor of 50 with respect to Q_0 . However, away from MPR, the resonance frequencies converge to the resonance frequency of the empty cavity and Q -factors also converge to Q_0 . In figure 7(b) Q_0 was assumed to be 9100, therefore, the points marked with the letters (a) and (f) correspond to the Q -factors of a slightly perturbed cavity, while points (c) and (d)

correspond to the total Q -factors of the cavity at MPR (points c and d in figure 6(a)). It can be seen that the total Q -factors at the MPR points are larger than Q_0 because for the assumed value of $\Delta H = 0.25$ Oe, $Q_m > Q_0$ and the conductor losses can be neglected there, since $Q_c \sim 50 Q_0$. This is a similar situation to that for very low loss whispering gallery mode dielectric resonators situated in a metal cavity when the total Q -factors can approach extremely large values.

When the size of a spherical sample increases the resonance condition changes as shown in figure 7(c). The continuous lines in figure 7(c) correspond to the rigorous solutions of the TDE (12) for the TE₁₀₁ mode of a spherical gyromagnetic resonator in free space, while the broken lines correspond to formula (19) which was derived independently by Hurd [38] and Marcereau [39]

$$w - H_{0r} = \frac{1}{3} - \frac{1}{90} (\varepsilon_f + 5) \left(2\pi \frac{d}{\lambda} \right)^2 = \frac{1}{3} - \frac{4\pi^2}{90} (\varepsilon_f + 5) \left(\frac{d}{\lambda} \right)^2. \quad (19)$$

It is seen that for moderately sized samples ($d/\lambda < 0.1$) the resonance conditions determined from formula (19) and from solutions to the TDE are very similar. Usually the effective g -factor of ferrite materials is determined from measurements of the MPR frequency for a given fixed static magnetic field value, therefore, d/λ corrections should be taken into account for its precise determination. The influence of metal enclosure on the MPR resonance frequency has been analyzed in [27].

Resonance phenomena in experiments with gyromagnetic samples are observed not at the FMR frequency when $w = H_{0r}$ but on one of many electrodynamic resonances in the gyromagnetic samples that are used in experiments. In several cases, that have been considered in this section, these resonances can be rigorously analyzed by employing an electrodynamic (ED) approach. An ED approach allows one to determine several parameters that cannot be analyzed using the magnetostatic theory. The most important of these are: (a) Q -factors depending on magnetic, dielectric, radiation and conductor losses. This is essential in determination of magnetic losses and in particular in measurements of the ferromagnetic linewidth, (b) resonance frequencies as functions of various parameters, such as the size of samples, their permittivity and the presence of metal enclosure.

4. Experiments

In this section experimental fixtures and the results of measurements of the complex permittivity, the initial permeability, permeability tensor and ferromagnetic linewidth of various gyromagnetic materials are presented.

4.1. Measurements of permittivity and the initial permeability below the frequency of natural ferromagnetic resonance (NFMR)

Transmission/reflection methods are based on measurements of transmitted and reflected electromagnetic power from a sample under test conditions illuminated by a well-determined incident electromagnetic wave. If the material of the sample is isotropic then determination of the complex permittivity and the complex permeability is possible from two measured

parameters: the complex reflection (S_{11}) and the complex transmission (S_{21}) coefficients. Broad frequency measurements of the complex permittivity and the initial complex permeability are usually performed in measurement cells made as a short section of a coaxial line or waveguide. In the determination of material properties, one has to know the relationship between the complex reflection and the complex transmission coefficients, the dimensions of the cell and sample, and the complex permittivity and complex permeability of the sample. Rigorous equations are available when a sample under test occupies the whole cross section between two planes perpendicular to the transmission line. The published standard methods for the transmission line techniques [40–42] present the full procedure for transmission line measurements in waveguides and coaxial lines. Papers [43, 44] present an explicit algorithm for permittivity/permeability determination. As an alternative, an iterative algorithm is presented in [45].

Results of measurements of permeability and permittivity using the transmission/reflection method in 7 and 14 mm coaxial air lines performed on the same samples in several laboratories have been described in NIST Technical Note [46]. Permittivity results presented in [46] for the same sample exhibited almost constant values up to 5 GHz but the results varied from one lab to another, probably due to the presence of air gaps. The imaginary parts of the permittivity for this sample were too small to be measured with reasonable accuracy. Conclusions from this report are as follows. Transmission/reflection measurements in waveguides and coaxial lines allow measurements of the initial complex permeability at a frequency range below the natural frequency of the FMR (NFMR) where ferrite materials exhibit substantial magnetic losses and relatively large permeability. The imaginary parts of permittivity and permeability can be measured with absolute resolution to the order of ± 0.02 , and the real parts with the relative uncertainties the order of a few percent. Therefore, transmission/reflection methods are suitable for measurements of lossy magnetic materials, particularly microwave absorbers, but they fail for measurements of low loss ferrites above the NFMR frequency. Results of the initial permeability measurements for a polycrystalline YIG sample employing a transmission/reflection method in a 7 mm coaxial line, reproduced from publication [47], are presented in figure 8. As shown in figure 8 there are two maxima of the imaginary part of the permeability. The first one at about 10 MHz is associated with the domain wall resonance and the second, at about 240 MHz, with the gyromagnetic resonance in the effective crystal anisotropy field. The NFMR frequency ($f_m = \gamma M_s$) of YIG is about 4.9 GHz. Above this frequency the imaginary part of the initial permeability is close to zero. This is the range of frequencies where circulators, isolators and phase shifters operate. Accurate measurements of the initial complex permeability and the complex permittivity at frequencies that are larger than the NFMR frequency are usually performed by employing various resonance methods.

4.2. Measurements of permittivity and the initial permeability above the frequency of NFMR

One of the most frequently used methods for the complex permittivity measurements of microwave ferrites is the cylindrical TM₀₁₀ mode resonator technique (figure 2(a)).

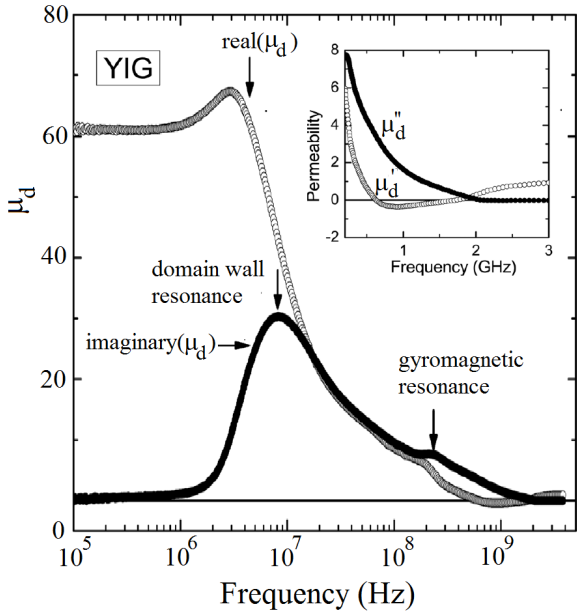


Figure 8. Results of the initial permeability measurements on toroidal polycrystalline YIG samples with an external diameter of 7 mm and thickness ~ 1.0 mm in 7 mm coaxial air lines. Gyromagnetic resonance frequency in the effective anisotropy field is about 250 MHz (for $H_a = 6.94$ kA m $^{-1}$). © Reprinted from [47], with the permission of AIP Publishing.

For these types of oscillations the electric field only has an axial component, which approaches maximum on the resonator axis. The method has been described in [48], and the standards in [49] and in most of them perturbation theory is employed to determine the relationship between the measured complex resonance frequency and the complex permittivity. The method allows determination of the real part of the permittivity with accuracy in the order of 1%–2%. The dielectric loss tangent resolution is in the order of $\pm 10^{-4}$. It is important to note that precise measurements require mitigation of air gaps between the sample and metal cavity walls and they should be performed at a frequency which is substantially larger than the frequency of NFMR. For materials with large saturation magnetization it is necessary to apply a static magnetic field bias to mitigate the influence of the magnetic properties of the sample on the measurement result. As shown in figure 4(a), the resonance frequency shift of the TM₀₁₀ mode resonator can be considered as being predominantly dependent on the dielectric properties of the sample for $H_{0r} > 1.6$. As already discussed, one of the most accurate methods for permittivity measurements is Courtney's method [29] where the sample being tested creates a dielectric-type resonator (as in figure 2(b)). With this method it is possible to measure the real part of the permittivity with accuracy in the order of 0.5% with the dielectric loss tangent resolution in the order of $\pm 2 \times 10^{-5}$. However, it should be pointed out that a strong electromagnet is necessary to mitigate the influence of the permeability of the sample on the determined permittivity value, particularly for samples with a larger aspect ratio (D/L) [50].

Advances in numerical computations of electromagnetic fields have enabled the implementation of resonant structures for measurements of samples with specific shapes and dimensions. The split post dielectric resonator (SPDR) depicted in figure 9(b), is one example of such an approach as it has been developed specifically for measurement of laminar dielectrics but it can be also used for measurements of the complex permittivity of ferrite substrates. When the single post dielectric resonator (SiPDR) operating on a similar frequency is also used, and a static magnetic bias is applied along the resonator's axis, then it is possible to determine the complex permittivity, and initial permeabilities, both perpendicular and parallel to the surface of the sample [50]. The SiPDR shown in figure 9(a) is intended for measurements of the initial permeability in the plane of the substrate. The other two SPDRs (figures 9(b) and (c)) are intended for measurements of the initial permeability in the direction perpendicular to the substrate, and for measurements of permittivity, when a sufficiently strong static magnetic field is applied along the axis of symmetry of the SPDRs. Results of the initial permeability measurements employing three sets of SPDRs and SiPDRs are presented in figure 10. More details concerning the measurements can be found in [50, 51]. As shown in figure 10, the initial permeability measured in the plane of a thin ferrite slab (substrate) is substantially smaller than the initial permeability measured in the direction perpendicular to the slab. The first permeability is smaller, while the second is larger than the theoretical value determined from the Schlömann model (8). As shown in figure 10(b), magnetic losses exponentially increase when the frequency becomes smaller than the frequency of NFMR (when $f/f_m < 1$).

In [52] one can find results of the initial permeability measurements on several small cylindrical rod shape samples measured in cylindrical TE₀₁₁ mode dielectric resonators, as shown in figure 2(c). Results of experiments have shown that the initial permeability values for some samples were smaller than the theoretical values predicted by the Schlömann model. One can conclude that the magnetic domain structure in demagnetized ferrite substrates is such, that the domain walls are mostly parallel to the plane of the substrate. Similarly, for demagnetized rods, the domain walls are mostly parallel to the axis of the rod. For this reason, the initial permeability exhibits sample shape-dependent magnetic anisotropy.

4.3. Measurement of the permeability tensor

In the past, the complex permeability tensor components have been measured by employing various resonant cavity techniques [47, 48, 53–61]. The most frequently used were cylindrical or rectangular degenerate mode cavities. Samples being tested typically had some form of sphere, cylindrical rod or rectangular slab situated in specific areas of the cavity where some of the electromagnetic field components vanish and some approach maxima. In most of these methods the external permeability concept and perturbation theory were employed for determination of the permeability components. Perturbation formulae for cylindrical and rectangular cavities

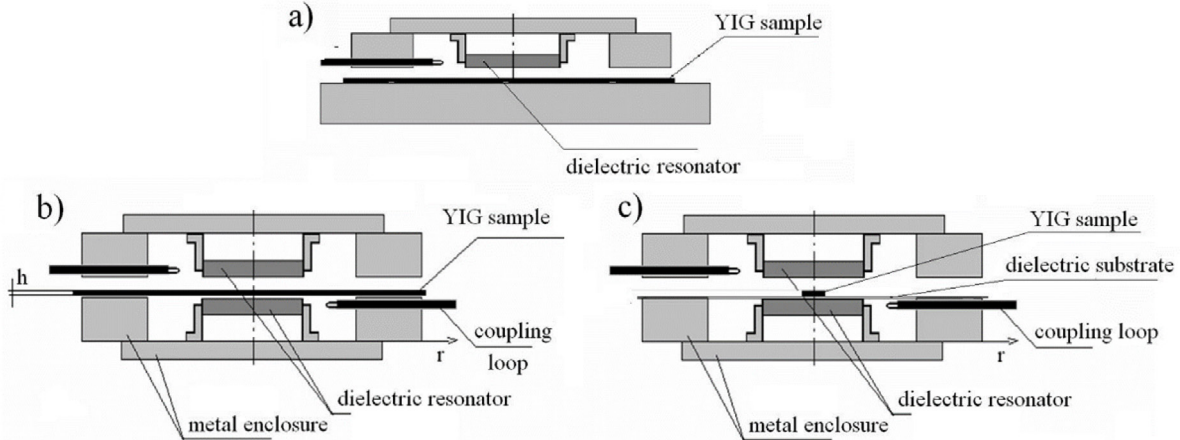


Figure 9. Schematic diagrams of resonators for measurements of ferrite substrates (a) a single post dielectric resonator where the sample is situated at a maximum magnetic field tangential to the sample, (b) a split post dielectric resonator where the sample is situated at a maximum electric field tangential to the sample and a maximum magnetic field normal to the sample, (c) a split post dielectric resonator where the small sample is situated at a maximum magnetic field normal to the sample.

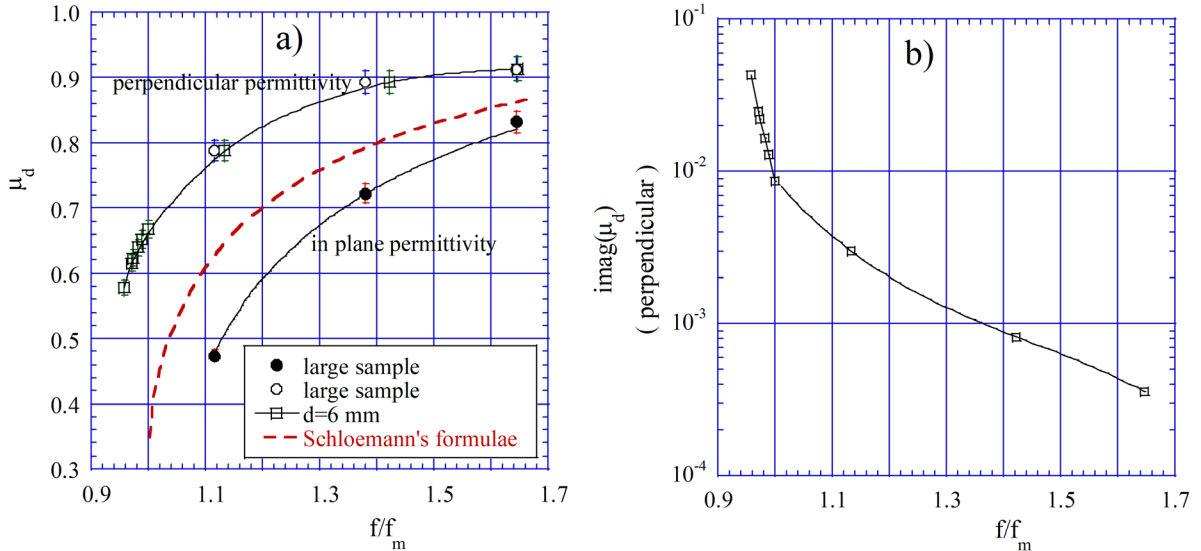


Figure 10. (a) Permeability components perpendicular and parallel to polycrystalline YIG substrates with a thickness of 0.383 mm and measured in single post and split post dielectric resonators, (b) the imaginary part of the initial permeability in the direction perpendicular to the substrate.

can be found in many papers and books, e.g. [3]. As has been already discussed, perturbation methods can be used when perturbation is small, but they introduce smaller or larger systematic errors and do not take into account dispersion of permeability. For this reason, rigorous methods of computations are preferred. The cylindrical TM_{nm0} mode cavity containing a cylindrical rod sample, was one of the first fixtures for which a rigorous electrodynamic approach (TDE) was used for determination of permeability tensor components [30]. Later, Muller-Gronau [25] and Le Roux [26] solved real TDE for TM_{nm0} modes to determine the real parts of the effective permeability tensor components.

In [23] a measurement method of all permeability tensor components based on rigorous solution of a TDE for the resonance structure which is shown in figure 2(c) was used. The measurements cell, which is shown in figure 2(c), uses three different modes in two dielectric resonators with the same

height and internal diameter but different external diameters. The larger dielectric resonator operates in the TE_{011} mode while the smaller operates in the HE_{111} mode. The external diameter of the smaller resonator is chosen such that its HE_{111} mode resonant frequency (with the sample but without any bias) is approximately the same as the TE_{011} mode resonant frequency of the larger resonator. Two resonators were used in order to reduce the influence of frequency on the measurement results (in such a situation the scaling of the permeability components with frequency is smaller). Without any bias the HE_{111} mode is degenerated; however, due to imperfect axial symmetry of the resonance structure, the two modes are split by a few MHz which gives rise to the measurement uncertainties. In the presence of static magnetic field bias, mode degeneracy is removed and two circularly polarized HE_{111}^- , HE_{111}^+ are present. As the off-diagonal component increases the frequency difference between the two modes also increases as

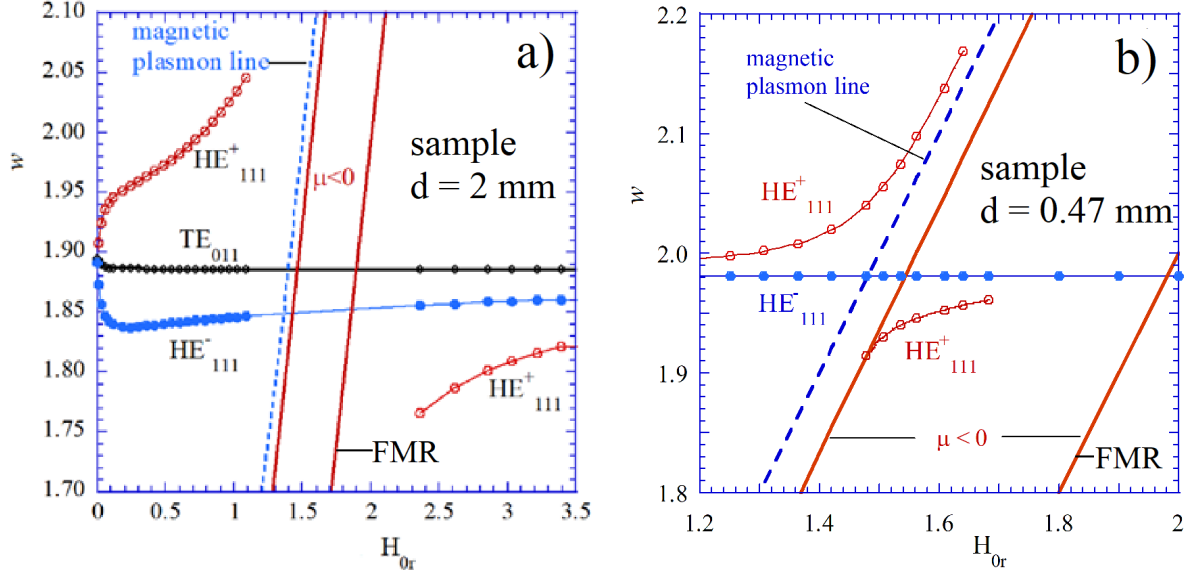


Figure 11. Normalized resonance frequencies versus a normalized static internal magnetic field for polycrystalline YIG samples measured in cylindrical dielectric alumina resonators shown in figure 2(c) (a) for a YIG sample with a diameter of 2 mm (b) for a YIG sample with a diameter of 0.47 mm. © 2018 IEEE: reprinted with permission from [37].

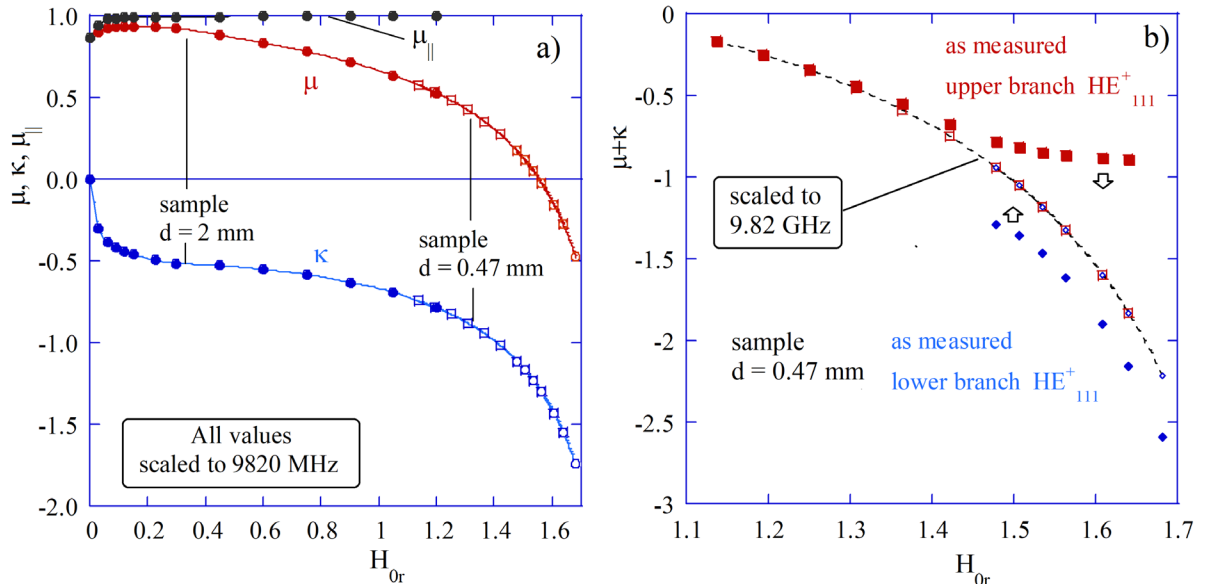


Figure 12. (a) Permeability tensor components of polycrystalline YIG samples versus static magnetic field bias determined from measurement data shown in figure 11. (b) The effective permeability for circularly polarized mode.

shown in figure 11(a). At zero bias the resonant frequencies of the degenerated HE_{111} mode and the TE_{011} mode depend only on the initial permeability and the scalar permittivity, so that the two unknowns can be determined from the system of two TDEs. When permittivity is known the three permeability tensor components can be determined at a fixed bias, from three measured frequencies, by solving the system of three TDEs for the HE_{111} , HE^+_{111} and TE_{011} modes. As shown in figure 11(a), experimental points are missing at the range of large absorption which is broad for the sample of 2 mm diameter. Additional experiments have been performed on the YIG sample having a diameter of 0.47 mm (volume about 18 times smaller than for the 2 mm sample) made of the same batch of material as the larger sample. Results of these experiments

are shown in figure 11(b). For the small sample, it can be seen that two branches of the HE^+_{111} mode are present in the range $1.48 < H_{0r} < 1.8$. From the measured resonance frequencies on these branches the sum of $\mu + \kappa$ can be determined as shown in figure 12(b). It should be noted that such determined values, at a fixed bias, are different, because the corresponding frequencies on the two branches are different. However, if frequency scaling is performed (one can assume that $\mu + \kappa = 1 + 1/(H_{0r} - w)$ for the lossless case), the results of the experiments overlap as shown in figure 12(b). The difference $\mu - \kappa$ can be determined from measured frequencies of the HE^-_{111} mode. In figure 12(a) results of determinations of all permeability tensor components are shown for the two samples. One should note that the value

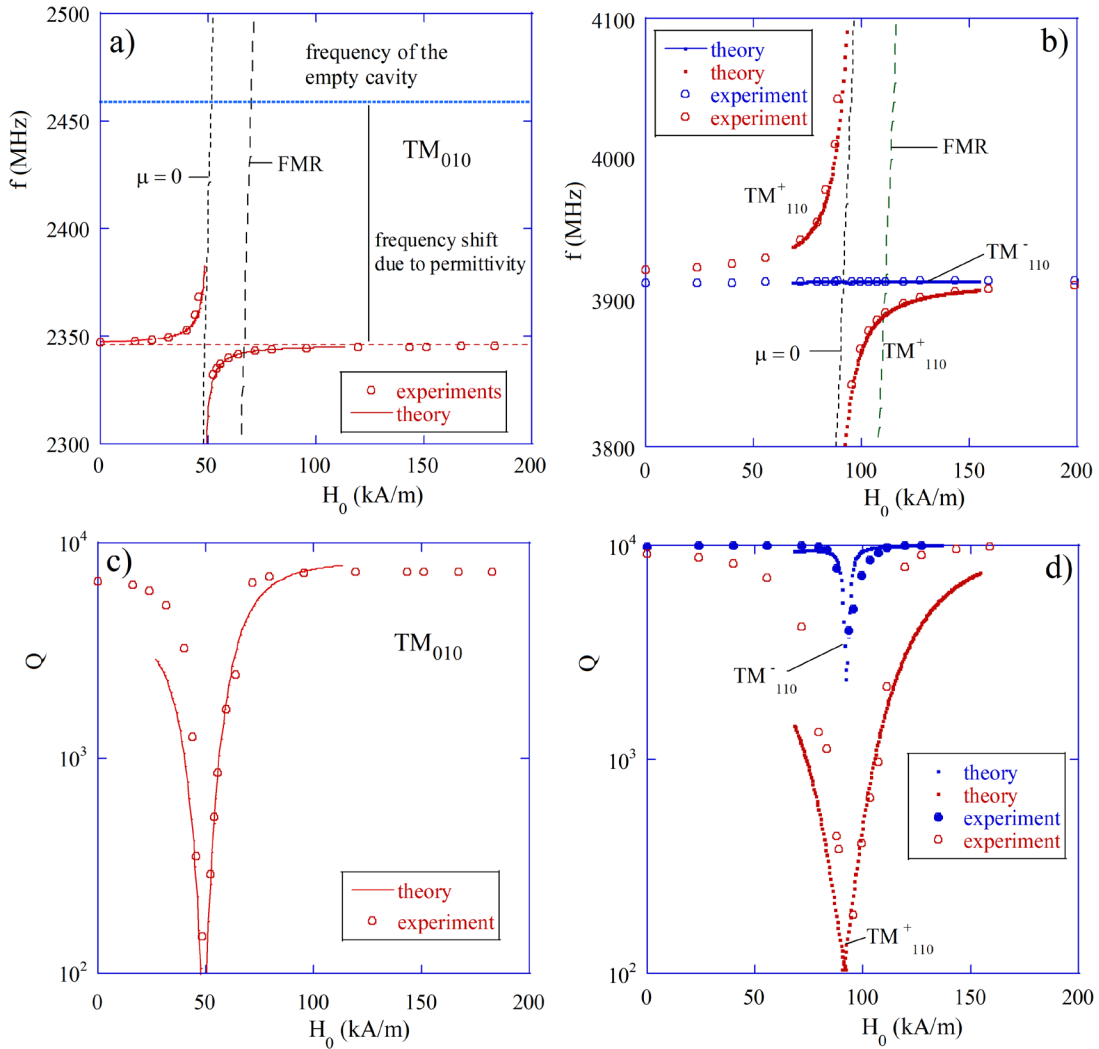


Figure 13. (a) Results of the resonance frequency measurements employing the TM_{010} mode. (b) Results of the resonance frequency measurements employing the TM_{110} mode. (c) Results of Q -factor measurements employing the TM_{010} mode. (d) Results of Q -factor measurements employing the TM_{110} mode. Dimensions of the cavity and the sample: $R_1 = 1.98$ mm, $R_2 = 46.67$ mm, $L = 30$ mm. $Q_0 = 8293$ (for the TM_{010} mode) and $Q_0 = 10209$ (for the TM_{110} mode). Sample G-510 (Trans-Tech) with $M_S = 43$ kA m $^{-1}$ and $\epsilon_f = 14.3$. Theoretical Q -factor values are computed for $\Delta H = 20$ Oe under the assumption $Q_c = Q_0$.

$\mu + \kappa = -1$ corresponds to the condition for the MPR in the cylindrical sample (magnetic plasmon lines are marked in figures 11(a) and (b)). This is one of the asymptotic lines for hybrid HE or EH modes in cylindrical samples. Other resonance lines for HE or EH modes are situated near the asymptote $w = \sqrt{H_{0r}(H_{0r} + 1)}$.

More details, including the results of measurements of the imaginary parts of permeability tensor components can be found in [23, 37]. Measurement uncertainties for real permeability components using this technique are typically in the order of 1% and the magnetic loss resolution is about 5×10^{-5} . As shown in figure 12, measured values of permeability tensor components agree very well with theoretical models described by formulae (2)–(4) for fully magnetized samples when $H_{0r} > 1$. Therefore, measurements of the individual tensor components are the most significant for partially magnetized ferrites. For $H_{0r} > 1$ it is sufficient to measure only three parameters that describe the permeability tensor:

the saturation magnetization M_S , the gyromagnetic ratio g and the FMR linewidth ΔH . These parameters can be individually measured but it is also possible to determine them in a different way. Specifically, one can perform measurements of some parameters in a resonance or non-resonance fixture containing a gyromagnetic sample versus the static magnetic field bias and then fit the theoretical model, with some unknown parameters, to the experimental data by employing an optimization procedure. This can be performed for all structures for which a theoretical model is available. In [62, 63] results of measurements of the complex permittivity and permeability tensor components are presented obtained by a broadband permeability measurement method based on the full-wave electromagnetic analysis of a non-reciprocal transmission line. Optimization procedures were employed to numerically determine the permittivity and permeability tensor from the scattering matrix parameters of the measurement cell measured in broad frequency ranges.

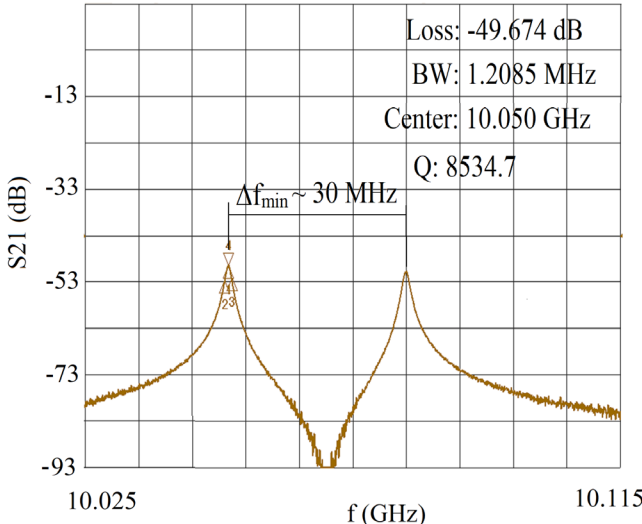


Figure 14. The scattering matrix coefficient $|S_{21}|$ versus frequency for a monocrystalline YIG sample (easy axis of YIG crystal [111] parallel to the external static magnetic field) with $R_1 = 0.25$ mm and $M_s \approx 140$ kA m $^{-1}$ measured in a rectangular cavity with a TE $_{102}$ mode resonance frequency equal to 10 050 MHz and $Q_0 = 9100$ (when empty). Reproduced from [28]. © IOP Publishing Ltd. All rights reserved.

In figure 13 results of measurements of the resonance frequencies and Q -factors versus static magnetic field bias for the TM $_{010}$ and TM $_{110}$ modes of a cylindrical cavity containing polycrystalline aluminium doped garnet are presented. For these modes the TDE is known (13) and one can fit parameters M_s , ΔH , ε_f in the TDE (13) to the experimental data.

The best fit is obtained for $M_s = 43$ kA m $^{-1}$, $\varepsilon_f = 14.3$ and $\Delta H \approx 20$ Oe. Discrepancies between the measured and theoretical Q -factor values in figures 13(c) and (d) are mainly due to simplified assumption in the theoretical model. For simplicity in the computations we assumed that the Q -factor due to conductor losses remains unchanged ($Q_c = Q_0$) while the near resonance Q_c can be significantly larger than Q_0 , as was shown in figure 7 for a spherical resonator.

One can observe that the resonance frequency shift due to permittivity for the TM $_{010}$ is large and almost constant for $H_0 > 3M_s$ (figure 13(a)). This means that permittivity of the sample can be uniquely determined from the measured resonance frequency shift of this mode at a sufficiently strong static magnetic field bias, as has been discussed earlier.

4.4. Measurements of ferromagnetic linewidth and the Gilbert damping factor

Ferromagnetic resonance linewidth and the Gilbert damping factor are some of the most important parameters of ferrites and metallic ferromagnetic films. The interest in the magnetization damping originates from the technological importance of the spin transfer and spin pumping effects. Usually these parameters are measured on samples with very small volumes, such as small spheres or thin ferromagnetic films. To obtain a noticeable effect of the sample on the parameters of a measurement setup it is necessary to excite one of the

magnon-type resonances in the sample. Measurement fixtures can be divided into resonance structures, such as metal cavities, dielectric, microstrip or stripline resonators and non-resonant structures, such as sections of different kinds of transmission lines (e.g. striplines and coplanar waveguides). A gyromagnetic sphere itself represents a magnon-type resonator that can be directly coupled to the ports of the automatic vector network analyzer (VNA). In view of the theoretical considerations presented in previous sections one would expect that measurable resonance effects would depend on the shape and size of the samples being tested. If the samples are very small, QMS theory allows one to predict Kittel's resonance condition, e.g. for these films the QMS resonance condition would be written as $w = \sqrt{H_{0r}(H_{0r} + 1)}$. For spherical samples several magnon resonances can be excited, but the MPR resonance (the mode of uniform precession in QMS nomenclature) has the largest magnitude.

The standard methods [49, 63, 64] of ΔH measurements of small spherical samples employ a rectangular metal cavity operating at a TE $_{10n}$ mode, where ' n ' is an even number. The background of these methods is based on the QMS theory and cavity perturbation technique. These standard methods are applicable for materials with $\Delta H > 10$ Oe. Employing an electrodynamic approach, it is possible to extend the FMR linewidth measurements on spherical samples in rectangular cavities to larger samples having arbitrary small ΔH values [28]. The method employs measurements of Q -factors with a VNA of two split MPR modes under such static magnetic field bias where the Q -factors become identical (points b and c) in figures 7(a) and (b).

Having known the diameter of the sample and its saturation magnetization ΔH values are evaluated using precomputed look-up tables. Typical measurement results for a monocrystalline YIG sample magnetized along the easy axis are shown in figure 14. From these measurement data the evaluated FMR linewidth value $\Delta H = 0.374$ Oe. One can note that the measured Q -factor values ($Q = 8534$) are only slightly smaller than the Q -factor of the empty cavity. If ΔH is smaller (e.g. 0.25 Oe) then the Q -factors would be larger than the Q -factor of the empty cavity, as shown in figure 7(b).

By employing this technique, several polycrystalline narrow linewidth materials with $\Delta H < 30$ Oe have been measured. We should remark that for small samples with a broader linewidth, the rigorous electrodynamic method and perturbation method overlap. The FMR linewidth of narrow linewidth gyromagnetic spheres can also be determined from direct Q -factor measurements of one of the magnon resonances, particularly the dominant MPR resonance. The measurement setup is depicted in the inset of figure 15(a). It consists of two orthogonal semi-loops and low loss sample support. If coupling coefficients are determined from the measured scattering matrix coefficients S_{11} , S_{22} and S_{21} , values and radiation losses are accounted for; the Q -factor due to magnetic losses can then be evaluated and $\Delta H = H_0/Q_m$. Such measurements were performed for MPR mode in a large frequency band for a monocrystalline YIG sample and the results are shown in figure 15(a). The theoretical unloaded Q -factor

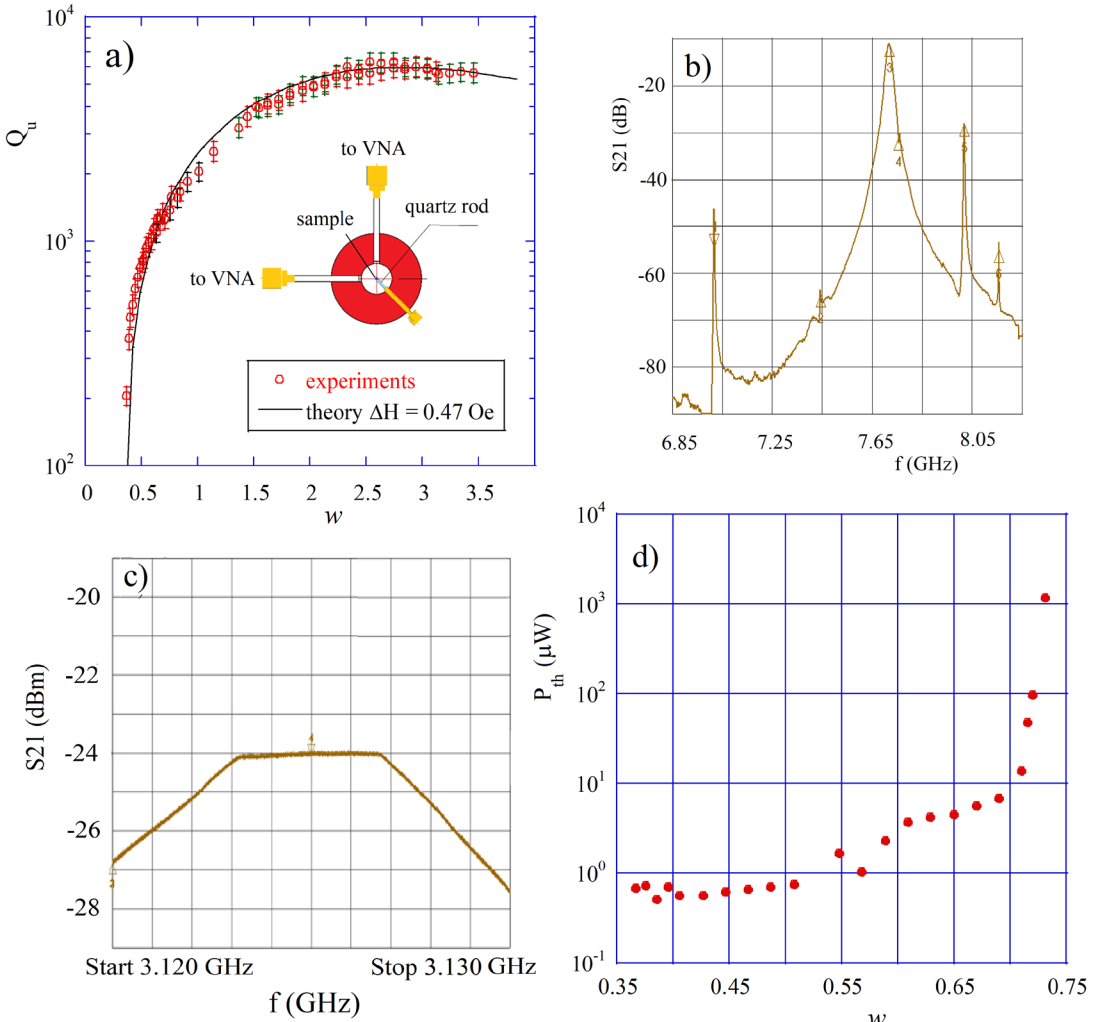


Figure 15. (a) The unloaded Q -factor of the MPR resonator as a function of the normalized static magnetic bias for a monocrystalline YIG sphere with a diameter of 0.5 mm coupled to a VNA via two orthogonal semi-loops, as shown in the inset of this figure, (b) multiple resonances for a strongly coupled YIG sphere, c) a resonance curve of MPR at $w = 0.63$ for a power level from a VNA about $10 \mu\text{W}$, (d) the threshold power level as a function of the normalized static magnetic bias for a monocrystalline YIG sphere. The easy magnetization axis of the YIG was oriented to be parallel to the applied static magnetic field.

values Q_u in figure 15(a) depend on the magnetic and radiation losses and they were obtained from solutions of (12) for $\Delta H = 0.59$ Oe. It should be mentioned, that according to the presented earlier theory, Q -factor limits for magnon modes are $\Delta H = H_0/Q_m$ for spherical, cylindrical and thin film samples. Therefore, one can expect the same Q -factor limits for other magnon modes in spherical samples. In figure 15(b) few resonances are shown that were measured on the sample from figure 15(a). It can be seen that the MPR mode has the largest magnitude because it is strongly coupled to the semi-loops. To determine its unloaded Q -factor S_{11} and S_{22} coefficients also have to be measured. Other modes are weakly coupled and their unloaded Q -factors can be directly measured (without corrections for coupling losses). The unloaded Q -factors for all measurable modes have very similar values. Therefore, one can alternatively determine FMR linewidth from Q -factor measurements in one of these modes. In [28] several spherical narrow linewidth samples were measured employing magnon–polariton modes in the TE_{011} mode

rectangular cavity and direct Q -factor measurements of MPR modes on these samples and results of the two methods agreed to within experimental uncertainties.

One important experimental issue should be considered when measurements are performed for a partially magnetized sample, i.e. for $H_0 < M_S$ (or $w < 2/3$). In this case, the power level delivered to the sample from the VNA should be sufficiently small to avoid Suhl instability. The Suhl instability [65, 66] is a well known phenomenon observed in experiments with the MPR mode. If the microwave power level exceeds some limit, higher order spin modes are generated and the MPR resonance resembles that in figure 15(c). One can say that it behaves like a power limiter. Theoretical studies revealed two processes responsible for this phenomenon. The parametric pumping process is referred to as the ‘first order Suhl instability’, and the second harmonic generation is called the ‘second order Suhl instability’. However, if the power levels from the VNA are reduced below some critical value (shown in figure 15(d)) then Lorentzian resonance curves are

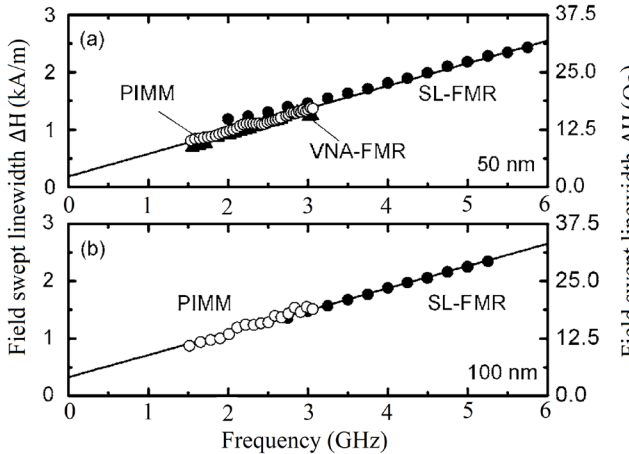


Figure 16. Comparison of the FMR linewidth results obtained from the stripline (SL), the vector network analyzer (VNA) and PIMM techniques on 50 and 100 nm Permalloy films. The solid circles are the SL-FMR results, the solid triangles are the VNA-FMR results and the open circles are the PIMM results. The solid lines are linear fits to all the points. Reprinted from [69] with the permission of AIP Publishing.

observed and their Q -factor can be measured. A large part of the experimental points in figure 15(a) (for $w < 2/3$) were measured with the reduced power levels.

Drawing figure 15(a) in linear scale one would observe that the measured unloaded Q -factors Q_u linearly depend on frequencies up to 11 GHz; therefore, in this range, the FMR linewidth determined as $\Delta H = H_0/Q_u$ is a constant quantity. For frequencies higher than 11 GHz, Q_u approaches maximum and it decreases above 15 GHz due to radiation losses [28] and possibly due to the ferromagnetic linewidth broadening with frequency as it takes place for thin metallic ferromagnetic films.

4.5. Non-resonant methods of FMR linewidth measurements employing transmission lines

For several decades the FMR linewidth has been measured by employing resonance techniques. The earliest researchers employed a swept static magnetic field method at a fixed frequency. Later, measurements were more often performed by sweeping the frequency at a fixed static magnetic field. Resonance techniques are generally more sensitive than non-resonance techniques, but they are restricted to a single frequency or to few frequencies on which the resonance system operates. Over the last two decades, due to the availability of VNAs, measurements have been commonly performed in frequency domains employing short sections of transmission lines, such as stripline or coplanar waveguides; although these methods have been known for about 50 years [67, 68]. Such an approach allows broad frequency band measurements: from hundreds of MHz to 30–40 GHz. The method which uses a stripline is referred to as broadband stripline FMR (BFMR) spectroscopy. Metallic ferromagnetic thin films are most frequently measured using one of these techniques. Hundreds of papers have been already published on these methods, e.g. [69–79]. Readers can find references to more than 200 papers

on this topic in [77]. In these methods the sample being tested, usually a thin film, deposited on a semi-insulating substrate, is placed on top of a transmission line and the scattering matrix parameters S_{11} , S_{22} and S_{21} of the line are measured with and without the static magnetic field bias. The static magnetic field is usually parallel to the surface of the sample and orthogonal to the microwave magnetic field of the transmission line. In some methods the static magnetic field is swept at a fixed frequency, while in others, a swept frequency technique is employed at a fixed static magnetic field [73]. There are also methods that involve the use of pulsed inductive microwave magnetometry (PIMM) [79]. Comparison of various FMR linewidth measurement methods in metallic thin films is well described in [69]. The authors of this paper employed the stripline (SL), the VNA and the PIMM technique for ferromagnetic linewidth measurements of thin Permalloy films. Results of their measurements are shown in figure 16 [69]. In the SL-FMR technique, a sweep of the static magnetic field was performed at several fixed frequencies, whereas in the VNA-FMR and PIMM techniques the frequency sweeps were performed at several fixed static magnetic fields. The results provided information showing that the linewidths measured by these three methods are consistent and that linewidths are a linear function of frequency for thin Permalloy films. This is different behavior than that for monocrystalline YIG samples where the FMR linewidth was almost constant up to 11 GHz.

It should be pointed out that radiation losses and conductor losses were not taken into account in FMR linewidth measurement of thin films.

5. Final remarks

Formal classification of permeability tensor and FMR linewidth measurement methods into resonance and non-resonance classes requires comment. For narrow linewidth samples, the samples themselves behave like tunable magnon-type resonators. Furthermore, they can be excited in different modes. The mode spectrum is the widest for spherical samples. Therefore, one can consider measurement fixtures as coupling systems to the magnon modes. In the simplest case such fixtures consist of two orthogonal loops; more complicated fixtures can be made as transmission lines or resonators.

Also, the segregation of measurement methods into frequency domains and the static magnetic field domain is not strict. In practice measurements are performed in two domains: static magnetic fieldfrequency domains, because gyromagnetic materials are dispersive. These days it has become common procedure to plot 2D mode spectra for experiments with gyromagnetic samples [80].

Something that is still a major problem in the determination of specific parameters, particularly FMR linewidth, is an appropriate theoretical model of magnon-type resonance which takes into account all the factors that would have an influence on the measurement results, such as radiation losses, conductor losses and coupling coefficients.

Although QMS and perturbation theories are, in many cases, sufficient for determination of the material properties

of gyromagnetic samples, for precise measurements of narrow linewidth materials, a rigorous electrodynamic approach is desirable, which has been shown in the theoretical part of this paper. Finally, it should be emphasized that in experiments with gyromagnetic samples, one does not measure permeability tensor components at FMR where the imaginary parts of the permeability tensor approach maxima, but rather at the static magnetic field—frequency points where some kind of magnon resonance appears, e.g. at MPR mode in spherical samples.

Acknowledgments

This work was supported by the TEAM-TECH project entitled ‘High-precision techniques of millimeter and sub-THz band characterization of materials for microelectronics’ operated within the Foundation for Polish Science TEAM-TECH Programme co-financed by the European Regional Development Fund, Operational Programme Smart Growth 2014–2020. I would like to thank P Aleshkevych, B Salski, P Kopyt and A Pacewicz for discussions on ferromagnetic resonance phenomena and for their help in some experiments presented in this paper.

ORCID iDs

Jerzy Krupka  <https://orcid.org/0000-0001-6393-1441>

References

- [1] Landau L D and Lifshitz E M 1935 On the theory of the dispersion of magnetic permeability in ferromagnetic bodies *Phys. Z. Sowjet.* **8** 153–64
- [2] Polder D 1949 On the theory of ferromagnetic resonance *Physica* **15** 253–5
- [3] Gurevich A G 1963 *Ferrites at Microwave Frequencies* (New York: Consultants Bureau Enterprises Inc.)
- [4] Schrömann E 1970 Microwave behavior of partially magnetized ferrites *J. Appl. Phys.* **41** 204–14
- [5] Cho H-S and Kim S-S 1999 M-hexaferrites with planar magnetic anisotropy and their application to high-frequency microwave absorbers *IEEE Trans. Magn.* **35** 3151–3
- [6] Meshram K N, Agrawal M R, Sinha B and Misra P S 2004 Characterization of M-type barium hexagonal ferrite-based wide band microwave absorber *J. Magn. Magn. Mater.* **271** 207–14
- [7] Seidel H and Boyet H 1957 Form of Polder tensor for single crystal ferrite with small cubic symmetry anisotropy energy *J. Appl. Phys.* **28** 452–4
- [8] Lee S, Grudichak S, Sklenar J, Tsai C C, Jang M, Yang Q, Zhang H and Ketterson J B 2016 Ferromagnetic resonance of a YIG film in the low frequency regime *J. Appl. Phys.* **120** 033905
- [9] Farle M 1998 Ferromagnetic resonance of ultrathin metallic layers *Rep. Prog. Phys.* **61** 755–826
- [10] Popov M, Zavisljak I, Ustinov A and Srinivasan G 2011 Sub-terahertz magnetic and dielectric excitations in hexagonal ferrites *IEEE Trans. Magn.* **47** 289–94
- [11] Lax B and Button K J 1962 *Microwave Ferrites and Ferrimagnetics* (New York: McGraw-Hill)
- [12] Osborn J A 1945 Demagnetizing factors of the general ellipsoids *Phys. Rev.* **67** 351–7
- [13] Chen D-X, Brug J A and Goldfarb R B 1991 Demagnetizing factors for cylinders *IEEE Trans. Magn.* **27** 3601–19
- [14] Baden-Fuller A J 1987 Ferrites at microwave frequencies, IEE electromagnetic wave series No 23, published by Peter Peregrinus (IEE)
- [15] Waldron R A 1963 Intrinsic and external permeabilities and susceptibilities of gyromagnetic materials *Br. J. Appl. Phys.* **14** 700–3
- [16] Kittel C 1948 On the theory of ferromagnetic resonance absorption *Phys. Rev.* **73** 155–61
- [17] Walker L R 1958 Resonant Modes of Ferromagnetic Spheroids *J. Appl. Phys.* **29** 318–23
- [18] Fletcher P C and Bell R O 1959 Ferrimagnetic resonance modes in spheres *J. Appl. Phys.* **30** 687
- [19] Joseph R I and Schrömann E 1961 Theory of magnetostatic modes in long, axially magnetized cylinders *J. Appl. Phys.* **32** 1001–5
- [20] Godtmann H D and Haas W 1967 Magnetodynamic modes in axially magnetized ferrite rods between two parallel conducting sheets *IEEE Trans. Microw. Theory Tech.* **15** 478–80
- [21] Kales L 1953 Modes in wave guides containing ferrites *J. Appl. Phys.* **24** 604–8
- [22] Epstein P S 1956 Theory of wave propagation in a gyromagnetic medium *Rev. Mod. Phys.* **28** 3–17
- [23] Krupka J 1991 Measurements of all permeability tensor components and the effective linewidth of microwave ferrites using dielectric ring resonators *IEEE Trans. Microw. Theory Tech.* **MTT-39** 1148–57
- [24] Bussey H E and Steinert L A 1957 An exact solution for a cylindrical cavity containing a gyromagnetic material *Proc. IRE* **45** 693–4
- [25] Muller-Gronau W and Wolff I 1983 A microwave method for the determination of the real parts of the magnetic and dielectric material parameters of the magnetized microwave ferrites *IEEE Trans. Instrum. Meas.* **32** 377–82
- [26] Le Roux P, Jecko F and Forterre G 1988 Nouvelle methode de determination des parties reelles des paramètres électriques et magnétiques des resonateurs à ferrites saturés et nonsaturés *Ann. Telecommun.* **43** 314–22
- [27] Krupka J, Aleshkevych P, Salski B, Kopyt P and Pacewicz A 2017 Ferromagnetic resonance revised-electrodynamic approach *Nat. Sci. Rep.* **7** 5750
- [28] Krupka J, Aleshkevych P, Salski B and Kopyt P 2018 Ferromagnetic linewidth measurements employing electrodynamic model of the magnetic plasmon resonance *Meas. Sci. Technol.* **29** 025501
- [29] Courtney W E 1970 Analysis and evaluation of a method of measuring the complex permittivity and permeability of microwave insulators *IEEE Trans. Microw. Theory Tech.* **18** 476–85
- [30] Bussey H E and Steinert L A 1958 Exact solution for a gyromagnetic sample and measurements on a ferrite *IRE Trans. Microw. Theory Tech.* **6** 72–6
- [31] Ilyinsky A S, Ya Slepian G and Ya Slepian A 1993 *Propagation, Scattering and Dissipation of Electromagnetic Waves* (London: Peter Peregrinus Ltd)
- [32] Agranovich V M and Ginzburg V L 1979 *Crystalooptics Considering Spatial Dispersion and Exciton Theory* (Moscow: Nauka)
- [33] Jackson J D 1999 *Classical Electrodynamics* 3rd edn (New York: Wiley)

- [34] Ruppin R 2002 Electromagnetic energy density in a dispersive and absorptive material *Phys. Lett. A* **299** 309–12
- [35] Vorobyev O B 2012 Energy density of macroscopic electric and magnetic fields in dispersive medium with losses *Prog. Electromagn. Res. B* **40** 343–60
- [36] Zheng X and Palfy-Muhoray P 2015 Electrical energy storage and dissipation in materials *Phys. Lett. A* **379** 1853–6
- [37] Krupka J, Aleshkevych P, Salski B and Kopyt P 2018 Magnetodynamic study of spin resonances in cylindrical and spherical YIG samples *IEEE Trans. Microw. Theory Tech.* **66** 803–12
- [38] Hurd R A 1958 The magnetic fields of a ferrite ellipsoid *Can. J. Phys.* **36** 1073–83
- [39] Marcereau J E 1959 Ferromagnetic resonance g factor to order *J. Appl. Phys.* **30** 184S–5S
- [40] ASTM Standard D 5568-95 1942 Standard test method for measuring relative complex permittivity and relative magnetic permeability for solid materials at microwave frequencies *1996 Annual Book of ASTM Standards (Electrical Insulation (II))* vol 10.02 (West Conshohocken, PA: ASTM)
- [41] ASTM Standard D5568-08 2009 Standard test method for measuring relative complex permittivity and relative magnetic permeability of solid materials at microwave frequencies using waveguide
- [42] UTE Standard 26-295 1999 Mesure de la permittivité et de la perméabilité de matériaux homogènes et isotropes à pertes dans le domaine des micro-ondes. Méthode de mesure en guide coaxial circulaire, UTE (Union Technique de l'Electricité et de la Communication), see C26-295, France (see www.ute-fr.com)
- [43] Nicholson A M and Ross G F 1970 Measurement of the intrinsic properties of materials by time domain techniques *IEEE Trans. Instrum. Meas.* **IM-19** 377–82
- [44] Weir W B 1974 Automatic measurement of complex dielectric constant and permeability at microwave frequencies *IEEE Proc.* **62** 33–6
- [45] Baker-Jarvis J R, Janezic M D, Grosvenor J H and Geyer R G 1992 Transmission/reflection and short-circuit line methods for measuring permittivity and permeability, NIST Technical Note 1355
- [46] Weil C M, Janezic M D and Vanzura E J 1977 Intercomparison of permeability and permittivity measurements using the transmission/reflection method in 7 and 14 mm coaxial air lines, NIST Technical Note 1386
- [47] Tsutaoka T, Kasagi T and Hatakeyama K 2011 Permeability spectra of yttrium iron garnet and its granular composite materials under dc magnetic field *J. Appl. Phys.* **110** 053909
- [48] Ogasawara N 1957 On the measurement of permittivity and tensor permeability of thin ferrite rods *Electrotech. J. Japan* **3** 126–30
- [49] IEC 556 1982
- [50] Krupka J, Gabelich S A, Derzakowski K and Pierce B M 1999 Comparison of split-post dielectric resonator and ferrite disk resonator techniques for microwave permittivity measurements of polycrystalline yttrium iron garnet *Meas. Sci. Technol.* **10** 1004–8
- [51] Derzakowski K and Krupka J 2010 Measurements of the complex permeability of yttrium iron garnet substrates near ferromagnetic resonance *Proc. of 18th Conf. on Microwave Radar and Wireless Communications MIKON 2010 (Vilnius, Lithuania, 14–16 June)* pp 1–3
- [52] Krupka J and Geyer R G 1996 Complex permeability of demagnetized microwave ferrites near and above gyromagnetic resonance *IEEE Trans. Magn.* **32** 1924–33
- [53] Artman J O and Tannenwald P E 1955 Measurement of susceptibility tensor in ferrites *J. Appl. Phys.* **26** 1124–32
- [54] Spencer E C, LeCraw R C and Reggia F 1956 Measurement of microwave dielectric constants and tensor permeabilities of ferrite spheres *Proc. IRE* **44** 790–800
- [55] Spencer E C, Ault L A and LeCraw R C 1956 Intrinsic tensor permeabilities on ferrite rods, spheres and disks *Proc. IRE* **44** 1311–7
- [56] Mash D and Nikolskij V V 1960 Measurement of the complex dielectric susceptibility and the magnetics susceptibility tensor of ferrites in the millimeter region *Sov. Phys.—Tech. Phys.* **4** 978–80
- [57] Green J J and Sandy F 1974 Microwave characterization of partially magnetized ferrites *IEEE Trans. Microw. Theory Tech.* **22** 641–5
- [58] Green J J and Sandy F 1974 A catalog of low power loss parameters and high power thresholds for partially magnetized ferrites *IEEE Trans. Microw. Theory Tech.* **22** 645–51
- [59] Schmidt L B, Harrington R D and Case W E 1967 Tensor permeability measurements at L-band frequencies using a degenerate mode cavity *J. Res. Natl Bur. Stand. C* **71C** 69–75
- [60] Srivastava C M and Roberts J 1958 Measurement of ferrite loss factors at 10 Gc s⁻¹ *Proc. Inst. Electr. Eng.* **105** 204–9
- [61] Quéffélec P, Le Floc'h M and Gelin P 2000 New method for determining the permeability tensor of magnetized ferrites in a wide frequency range *IEEE Trans. Microw. Theory Tech.* **48** 1344–50
- [62] Chevalier A, Cortes J, Lezaca J and Queffelec P 2013 Broadband permeability measurement method for ferrites at any magnetization state: experimental results *J. Appl. Phys.* **114** 174904
- [63] ASTM A883/A883M-01 Standard test method for ferrimagnetic resonance linewidth and gyromagnetic ratio of nonmetallic magnetic materials
- [64] IS 8426:2001 2001 Indian standard measuring methods for properties of gyromagnetic materials intended for application at microwave frequencies
- [65] Anderson P W and Suhl H 1955 Instability in the motion of ferromagnets at high microwave power levels *Phys. Rev.* **100** 1788
- [66] Suhl H 1957 The theory of ferromagnetic resonance at high signal powers *J. Phys. Chem. Solids* **1** 209–27
- [67] Waldron R A 1964 Theory of a stripline cavity for measurement of dielectric constants and gyromagnetic resonance linewidths *IEEE Trans. Microw. Theory Tech.* **12** 123–31
- [68] Maxwell S P 1966 A stripline cavity resonator for measurement of ferrites *Microw. J.* **9** 99–102
- [69] Kalarickal S S, Krivosik P, Wu M, Patton C E, Schneider M L, Kabos P, Silva T J and Nibarger J P 2006 Ferromagnetic resonance linewidth in metallic thin films: comparison of measurement methods *J. Appl. Phys.* **99** 093909
- [70] Sokolov A S, Geiler M and Harris V G 2016 Broadband ferromagnetic resonance linewidth measurement by a microstripline transmission resonator *Appl. Phys. Lett.* **108** 172408
- [71] Sievers S, Kurda J, Liebing N, Hohls F and Schumacher H W 2017 Microwave interferometry for high sensitivity VNA-FMR measurements *IEEE Trans. Magn.* **53** 1–4
- [72] Neudecker I, Woltersdorf G, Heinrich B, Okuno T, Gubbiotti G and Back C H 2006 Comparison of frequency, field, and time domain ferromagnetic resonance methods *J. Magn. Magn. Mater.* **307** 148–56

- [73] Bilzer C, Devolder T, Crozat P and Chappert C 2008 Open-circuit one-port network analyzer ferromagnetic resonance *IEEE Trans. Magn.* **44** 3265–8
- [74] Barry W 1986 A broad-band, automated, stripline technique for the simultaneous measurement of complex permittivity and permeability *IEEE Trans. Microw. Theory Tech. MTT-34* 80–4
- [75] Silva T J, Lee C S, Crawford T M and Rogers C T 1999 Inductive measurement of ultrafast magnetization dynamics in thin-film Permalloy *J. Appl. Phys.* **85** 7849–62
- [76] Bilzer C, Devolder T, Crozat P, Chappert C, Cardoso S and Freitas P P 2007 Vector network analyzer ferromagnetic resonance of thin films on coplanar waveguides: comparison of different evaluation methods *J. Appl. Phys.* **101** 074505
- [77] Maksymov S and Kostylev M 2015 Broadband stripline ferromagnetic resonance spectroscopy of ferromagnetic films, multilayers and nanostructures *Physica E* **69** 253–93
- [78] Heinrich B, Cochran J F and Hasegawa R 1985 FMR line broadening in metals due to two-magnon scattering *J. Appl. Phys.* **57** 3690
- [79] Kos A B, Silva T J and Kabos P 2002 Pulsed inductive microwave magnetometer *Rev. Sci. Instrum.* **73** 3563–9
- [80] Bourhill J, Kostylev N, Goryachev M, Creedon D L and Tobar M E 2015 Ultra-high cooperativity interactions between magnons and resonant photons in a YIG sphere (arXiv:[1512.07773v2\[quant-ph\]](https://arxiv.org/abs/1512.07773v2))